

Innovative repair of corroded marine plates under buckling



Nasos Biniaris

National Technical University of Athens
School of Naval Architecture and Marine Engineering
Shipbuilding Technology Laboratory

Supervising professor

Konstantinos N. Anyfantis

Περίληψη

Η απώλεια υλικού λόγω ομοιόμορφης διάβρωσης μπορεί να οδηγήσει σε σημαντική μείωση της αντοχής μιας πλάκας σε λυγισμό, θέτοντας την πλάκα και τις περιβάλλουσες κατασκευές σε κίνδυνο αστοχίας. Αναλόγως με το μέγεθος των παραπάνω, η πλάκα είτε αντικαθίσταται είτε ενισχύεται με επικάλυψη άλλης πλάκας ή ενισχυτικών. Σε κάθε περίπτωση, θερμές εργασίες, όπως η συγκόλληση, είναι αναπόφευκτες.

Στη παρούσα εργασία εξετάζεται μία καινοτόμος μέθοδος επισκευής με την χρήση ενισχυτικών από σύνθετα υλικά. Το θεωρητικό υπόβαθρο που χρειάστηκε για την κατανόηση του προβλήματος της επισκευής από σύνθετα υλικά, το οποίο περιέχει τον λυγισμό πλακών και την μηχανική ανισοτροπικών υλικών, αναλύθηκε σε βάθος. Δημιουργήθηκε μοντέλο ανάλυσης πεπερασμένων στοιχείων με σκοπό να μελετηθεί η συμπεριφορά μίας μεταλλικής πλάκας με σύνθετη ενίσχυση σε γραμμικό ελαστικό λυγισμό. Οι προσομοιώσεις εξήγαγαν αποτελέσματα για πλάκες που υπόκεινται σε διαξονική θλίψη και καθαρή διάτμηση.

Μετά την εξαγωγή των αποτελεσμάτων, εργαλεία στατιστικής ανάλυσης όπως το Κεντρικό Οριακό Θεώρημα (ΚΟΘ), Central Composite Design (CCD) και Response Surface Methodology (RSM) χρησιμοποιήθηκαν με σκοπό να βελτιστοποιηθεί η διαδικασία σχεδίασης της επιδιόρθωσης και να δημιουργηθεί ένα πιθανοθεωρητικό μοντέλο που να καλύψει μία πληθώρα περιπτώσεων επιδιόρθωσης.

Abstract

Material wastage due to uniform corrosion can lead to significant reduction of the buckling capacity of a plate, putting the plate and its surrounding structures at risk of failure. Depending on the magnitude of the above, the plate is either replaced or reinforced with doubler plates or stiffeners. In both cases, hot works, like welding, are inevitable.

An innovative repair method with the use of composite beams is examined in this work. The theoretical background needed to understand the problem of composite reinforcement, including buckling of plates and mechanics of anisotropic materials, was analyzed in depth. A Finite Element Analysis (FEA) model was created in order to study the response of a metal plate with composite reinforcement in linear elastic buckling. The simulations extracted results for plates subjected to bi-axial compression and pure shear.

After the extraction of the results, statistical analysis tools like the Central Limit Theorem (CLT) Central Composite Design (CCD) and Response Surface Methodology (RSM) were utilized in order to optimize the repair design process and create a probabilistic model to cover a wide variety of repair cases.

Acknowledgements

First and foremost, I would like to express my gratitude to my professor Konstantinos Anyfantis who was always by my side when needed.

Then, I would like to thank my team in Salamis Shipyards for providing me with the necessary experience to connect my theoretical knowledge with the practical application.

Finally, I would like to thank my family and my girl for their continuous support throughout my studies.

Contents

1 Introduction.....	1
2 Theoretical background	4
2.1 Buckling of simply supported plates.....	4
2.1.1 Biaxial compression.....	4
2.1.2 Pure shear.....	8
2.2 Transversely isotropic materials	9
2.3 Finite Element Method	11
2.3.1 Shell elements	13
2.4 Statistical Analysis.....	15
2.4.1 Central Limit Theorem	15
2.4.2 Confidence intervals	15
2.4.3 Factorial design.....	17
2.4.4 Response surface methodology.....	18
2.4.5 Central composite design.....	19
3 Geometry and Simulation	20
3.1 FEM Modeling.....	22
3.1.1 Steel plate.....	22
3.1.2 FRP flange	22
3.1.3 FRP web.....	23
3.1.4 Steps.....	24
3.1.5 Loads, BCs and constraints.....	25
3.1.6 Post-processing	27
4 Numerical Results.....	28
4.1 Model verification.....	28
4.2 Simulations results.....	32
5 Probabilistic Approach.....	53
5.1 Model fitting	53
5.1.1 CCD	53
5.1.2 CLT	54
5.1.3 RSM.....	55
5.2 Model testing	57
6 Concluding Remarks.....	59
References.....	60

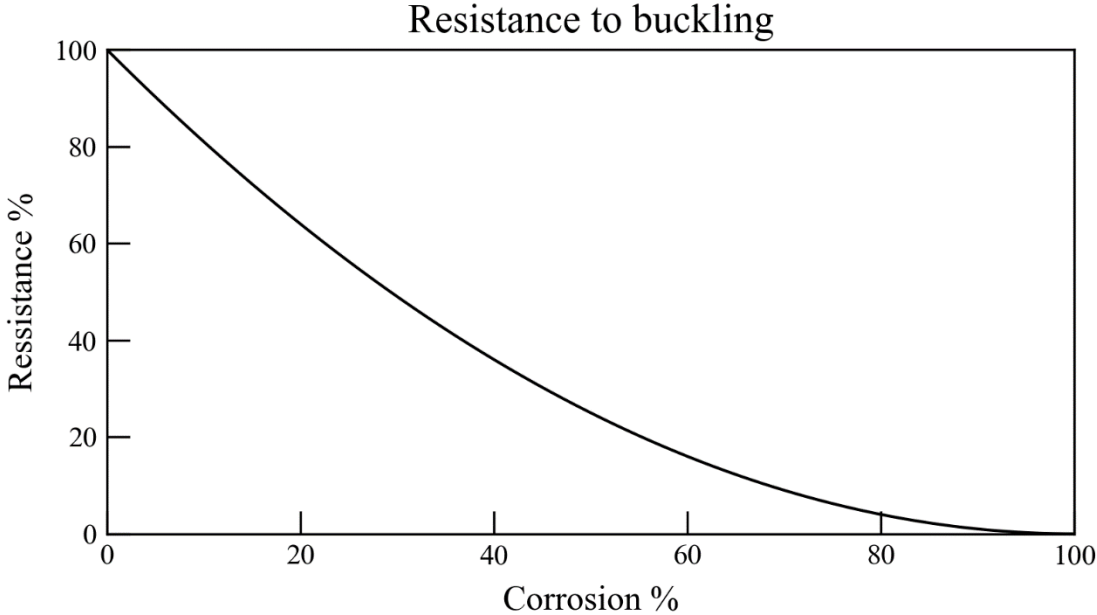
1 Introduction

Steel marine plates are one of the main structural components of a ship. Due to the extreme conditions the plates are subjected to (stresses, humid environments, seawater etc.), material wastage due to corrosion is inevitable in the ship's life (30 – 50 years). The usual corrosion types observed in marine plates are:

- Uniform corrosion
- Galvanic corrosion
- Pitting corrosion

Out of these types the most commonplace is uniform (or general) corrosion. Uniform corrosion leads to a uniform, on average, reduction of thickness to the affected plate. Although the ship's scantlings are designed with excess thickness to take into account this phenomenon (IACS [1]), in some cases, because of indeterminate factors, this isn't sufficient. If the plate is subjected to compressive or/and shear loads, material wastage due to corrosion can lead to the plate buckling in operation loads.

A plate's resistance to linear elastic buckling is analogous to the square of its thickness. If the thickness is reduced to 90% of the initial, the plate's resistance is reduced to 81%.



Every 5 years ships generally go under survey by a classification society, in which the ship is checked for structural deficiencies, such as:

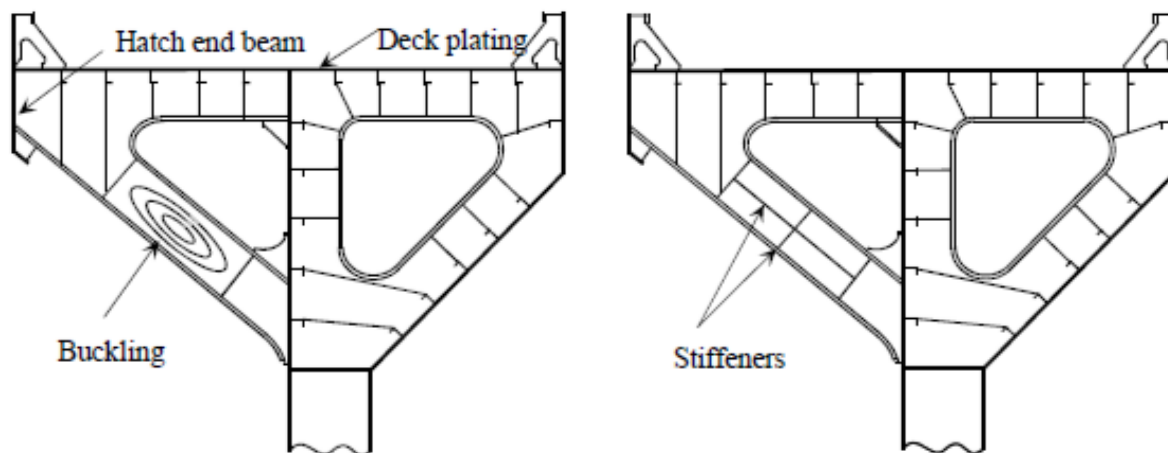
- Material wastage
- Fractures
- Deformations

In most cases where deformations are observed on a plate, IACS [2][3][4] suggests the repair solutions below:

- Fairing of the plate and reinforcement with doubler plate or stiffener, for small deformations and/or material wastage
- Removal of the plate and replacement with an insert plate of the same material for large deformations and/or material wastage

Hot work is inevitable for large deformations, because the buckled plate has to be cut-off (with plasma, oxygen & acetylene fuel, etc.) and a new one has to be welded in place. The same could be said for the small deformations case, the most common way to fair a deformed plate is with flame-straightening and the doubler plate or the stiffeners have then to be welded to the plate.

To do hot works in a compartment, a certificate of degassing (Gas Free) must be issued for the safety of the workers and the environment. Also hot works like cutting and welding, degrade the metal at the heat affected zone, which is why they should be avoided if possible.



[2]

The latest years, new methods have been proposed and studied [5][6] to replace these conventional repair methods, using composite materials (GFRP, CFRP, etc.). The proposed alternatives are:

- Adhesion of composite patches instead of the welding of doublers
- Adhesion of composite beams instead of the welding of stiffeners

These are short term repair methods, they can be imposed while the ship is on sail and the scope is to keep the plates in the safe zone until the ship's scheduled dry docking.

The main advantage of these repair methods is they can be carried out without hot work. The area of adhesion between metal and composite has to be cleaned and grinded, a layer of adhesive (epoxy resin, polyester resin etc.) is then to be applied at the area and the composite reinforcement is to be placed on the adhesive.

In this work, the repair of steel plates with the use of composite beams is analyzed using the Finite Element Analysis (FEA) program ABAQUS. The design is based on the plate's strength to linear elastic buckling in bi-axial compression and pure shear.

The reinforcement arrangement examined is end-to-end reinforcement with composite fiber reinforced plastic (FRP) T-beams with the flange placed on the plate to increase the area of adhesion. For the context of this work the assumptions listed below were made in order to simplify the problem:

- The repaired plate is completely straightened
- The material wastage is uniform
- The steel plate and the FRP beam are perfectly adhered to each other
- The steel plate, the FRP beam and the adhesive bondline are all in the linear elastic region

A number of FEA simulations were run to understand the nature of the composite reinforcements and their different arrangements on the same plate. Then, after reaching to conclusions about the optimal reinforcement arrangements, a probabilistic model was created and tested to extract results for plates with any dimension.

2 Theoretical background

2.1 Buckling of simply supported plates

The plate governing equation for buckling is:

$$D\nabla^4 w = p(x, y) + N_x \frac{\partial^2 w}{\partial x^2} + N_y \frac{\partial^2 w}{\partial y^2} + 2N_{xy} \frac{\partial^2 w}{\partial x \partial y}$$

where:

- $D = \frac{Et^3}{12(1-\nu^2)}$, the plate's flexural rigidity
- $p(x, y)$, the lateral pressure in N/m² units
- N_x, N_y, N_{xy} , the in-plane edge loads as shown in figure in N/m units

The boundary conditions of the plate is simple support, which means that the edges are free to rotate so the modes will consist of sine-waves.

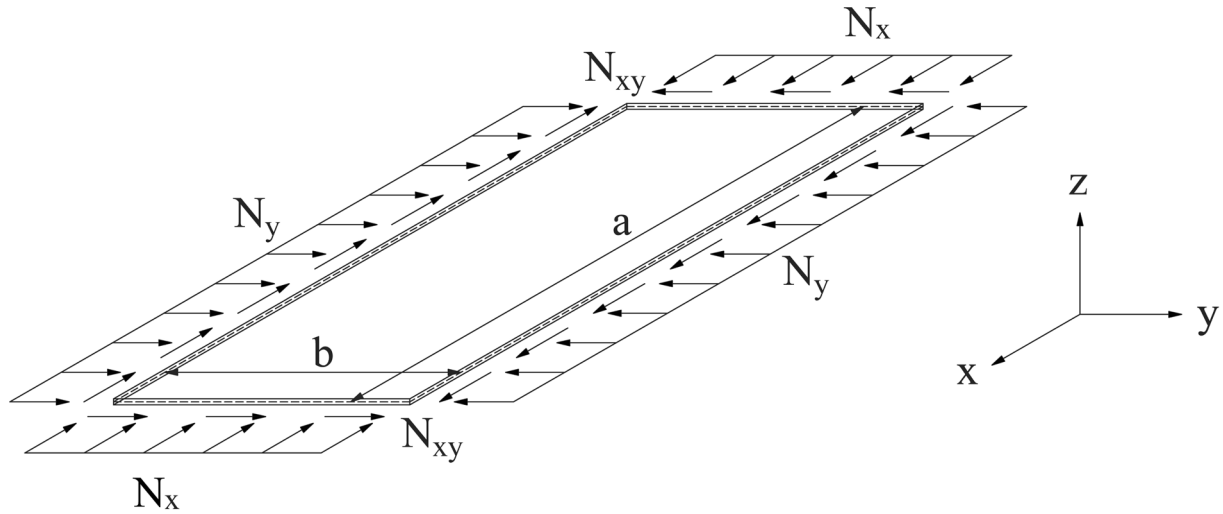


Figure 3. Plate coordinate system

2.1.1 Biaxial compression

For a simple-supported plate in biaxial compression, set $N_{xy} = p(x, y) = 0$. Assume the solution to be of the Navier form

$$w(x, y) = \sum_n \sum_m A_{nm} \sin \frac{m\pi x}{a} \sin \frac{n\pi y}{b}$$

and substitute it to the governing equation.

Set $\beta = N_y/N_x$ and $r = a/b$, the critical buckling load is

$$N_{x,cr} = K_C \frac{D\pi^2}{b^2}, \quad K_C = \min_{m,n} \left(\frac{[m^2 + n^2 r^2]^2}{r^2 [m^2 + \beta n^2 r^2]} \right)$$

Setting β between 0 and 1, the formula for K_C can still take into account all the possible cases by inverting β and r if needed (e.g. a plate with $r = 3$ and $\beta = 2$ is the same as a plate with $r = 1/3$ and $\beta = 1/2$). It will be proven that K_C minimizes only if $n = 1$ for β between $[0,1]$.

Consider the function $f = f(n)$

$$f(n) = \frac{[m^2 + n^2 r^2]^2}{r^2 [m^2 + \beta n^2 r^2]}$$

taking the first derivative

$$\frac{df}{dn} = \frac{2[m^2 + n^2 r^2][2nr^2]r^2[m^2 + \beta n^2 r^2] - r^2[2\beta nr^2][m^2 + n^2 r^2]^2}{r^4 [m^2 + \beta n^2 r^2]^2}$$

by simplifying we get that

$$\frac{df}{dn} = \frac{2n[m^2 + n^2 r^2]}{[m^2 + \beta n^2 r^2]^2} ([2 - \beta]m^2 + n^2 r^2 \beta)$$

which is always positive for β in $[0,1]$. The function f is strictly increasing with respect to n for every positive n , so the minimum of $f(n)$ is $f(1)$ since n is a natural number.

Replacing n with 1, the K_C formula simplifies

$$K_C = \min_m \left(\left[\frac{m}{r} + \frac{r}{m} \right]^2 \frac{m^2}{m^2 + \beta r^2} \right)$$

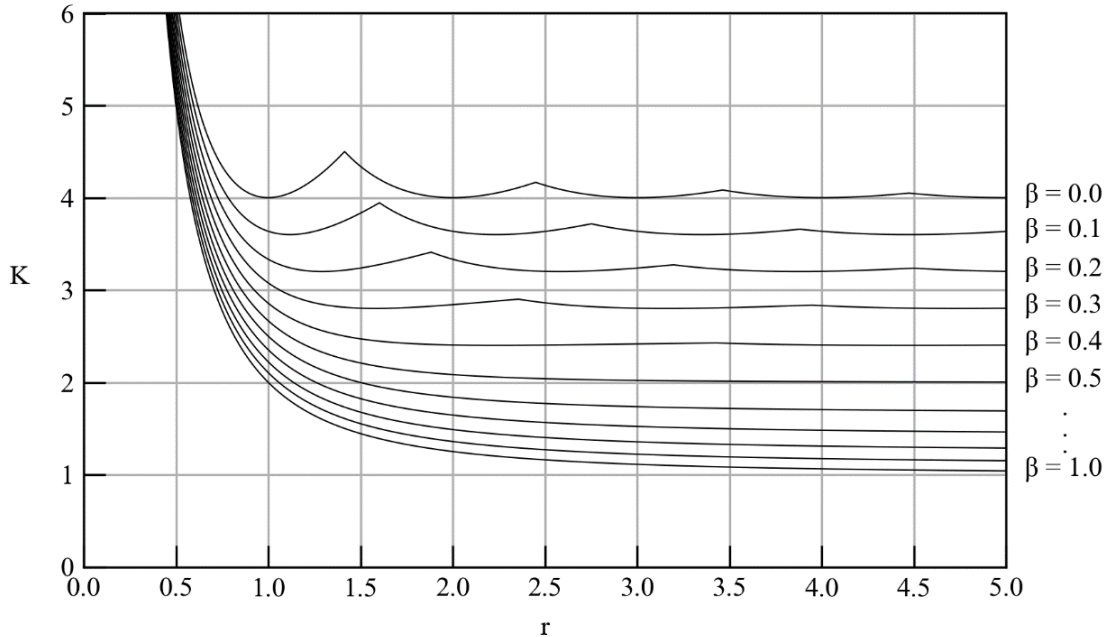


Figure 4. Buckling coefficient for plates in bi-axial compression

The above prove that a mode with multiple half-waves in both directions cannot exist for any plate in biaxial compression.

For the special case of $\beta = 0$, the plate is subjected to uniaxial compression and the formula below can be derived:

$$K_C = \min_m \left(\left[\frac{m}{r} + \frac{r}{m} \right]^2 \right)$$

It will be proven that K_C minimizes only if $m = 1$ for β between $[0.5, 1]$.

Consider the function $f = f(m)$

$$f(m) = \frac{[m^2 + r^2]^2}{r^2[m^2 + \beta r^2]}$$

taking the first derivative

$$\frac{df}{dm} = \frac{2[m^2 + r^2][2m]r^2[m^2 + \beta r^2] - r^2[2m][m^2 + r^2]^2}{r^4[m^2 + \beta r^2]^2}$$

by simplifying we get that

$$\frac{df}{dm} = \frac{2m[m^2 + r^2]}{r^2[m^2 + \beta r^2]^2} [m^2 + r^2(2\beta - 1)]$$

which is always positive for $\beta \geq 0.5$. The function f is strictly increasing with respect to m for every positive m , so the minimum of $f(m)$ is $f(1)$ since m is a natural number. These modes always have a single half-wave in both directions.

Replacing m with 1, the K_C formula simplifies

$$K_C = \left[\frac{1}{r} + r \right]^2 \frac{1}{1 + \beta r^2}, \quad \beta \geq 0.5$$

by taking the limit of K_C as r reaches infinity, we find that for long plates

$$K_{C_\infty} = \frac{1}{\beta}, \quad \beta \geq 0.5$$

If $\beta \leq 0.5$, the derivative of f with respect to r can be used to find the value of the minima of K_C which is also the value of convergence for long plates.

Take the function

$$f(r) = \frac{[m^2 + r^2]^2}{r^2[m^2 + \beta r^2]}$$

m and β are parameters. Change of variable

$$\frac{r^2}{m^2} = u > 0$$

Respecting the chain rule, proceed to find the minima

$$\frac{df}{dr} = \frac{df}{du} \cdot \frac{du}{dr} = 0$$

$$f(u) = \frac{[1+u]^2}{u+\beta u^2}, \quad \frac{df}{du} = \frac{2[1+u][u+\beta u^2] - [1+2\beta u][1+u]^2}{[u+\beta u^2]^2}, \quad \frac{du}{dr} = \frac{2r}{m^2} > 0$$

by simplifying

$$\frac{df}{du} = \frac{1+u}{[u+\beta u^2]^2} [u(1-2\beta) - 1] = 0 \rightarrow u(1-2\beta) - 1 = 0 \rightarrow u = \frac{1}{1-2\beta}$$

replacing u in f(u) we get

$$f(u) = 4(1-\beta)$$

This proves that the value of the minima is only dependent on the parameter β , which means that for long plates the buckling constant is

$$K_{C\infty} = 4(1-\beta), \quad \beta \leq 0.5$$

For the special case of $\beta = 1$, the plate is subjected to equi-biaxial compression. K_C simplifies to the form:

$$K_C = 1 + \frac{1}{r^2}$$

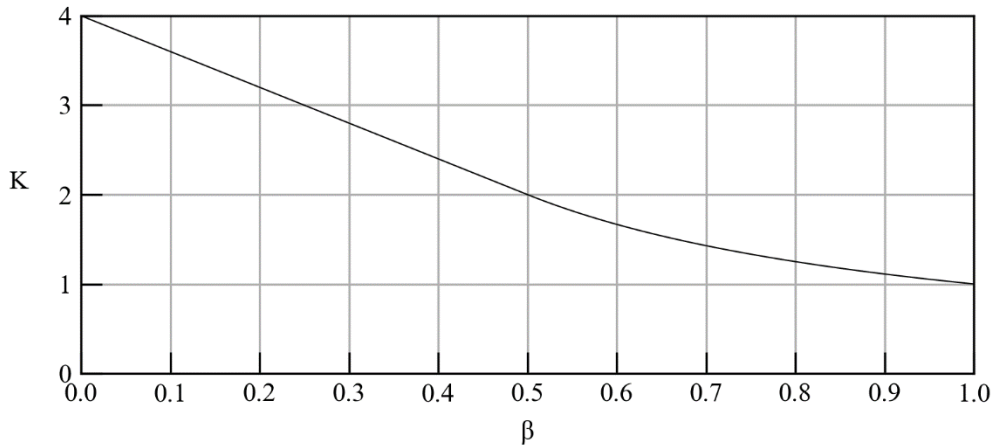


Figure 5. Buckling coefficient for long plates in bi-axial compression

2.1.2 Pure shear

For a hinged plate in pure shear set $N_x = N_y = p(x,y) = 0$. An analytical solution of the equation doesn't exist. Stein and Neff [7] calculated K_S through the use of matrix iteration method considering both the symmetric and the antisymmetric modes.

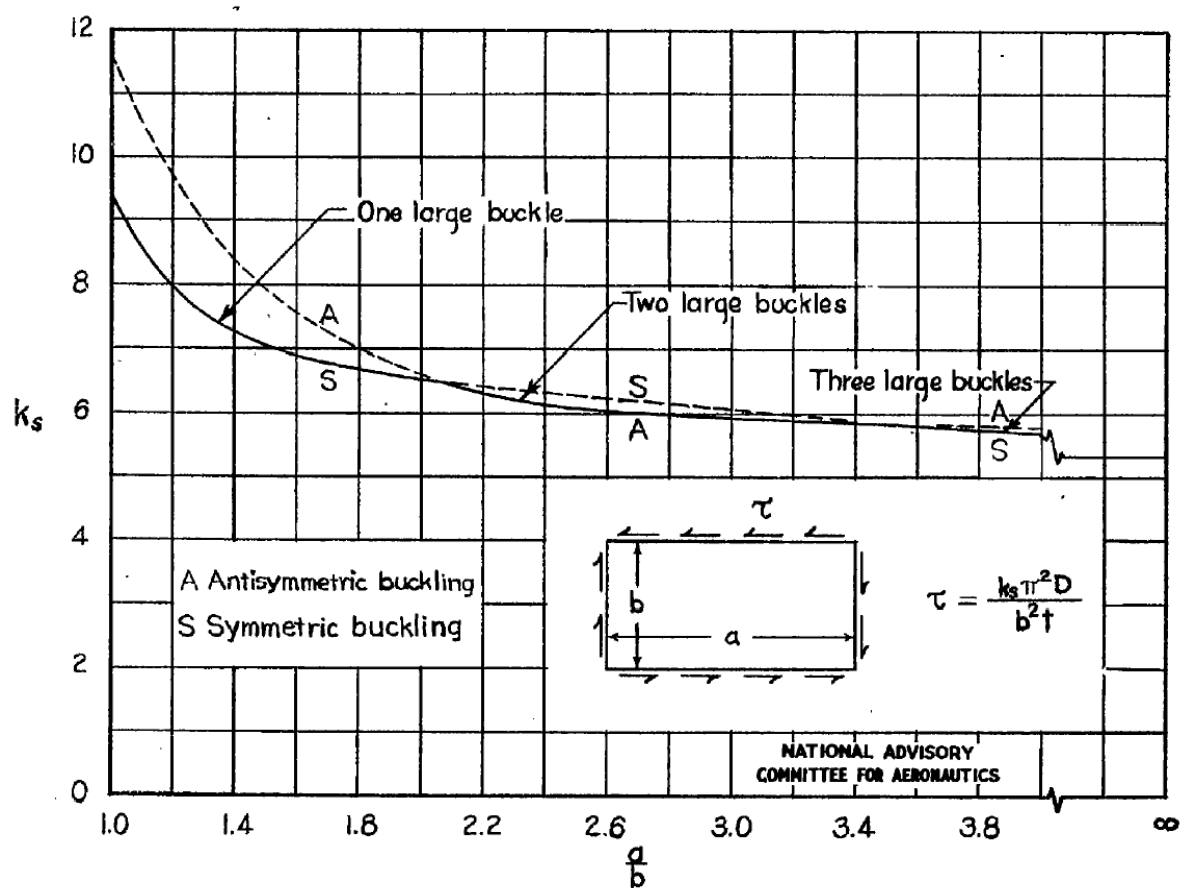


Figure 6. Buckling coefficient for plates in pure shear

The interpolation below is commonly used to calculate the value of K_S for long plates:

$$N_{xy,cr} = K_S \frac{D\pi^2}{b^2}, \quad K_S = \frac{4}{r^2} + 5.34, \quad r \geq 1.0$$

2.2 Transversely isotropic materials

Transversely isotropic materials represent a class of materials exhibiting directional dependence in their mechanical properties. Transversely isotropic materials are a subset of orthotropic materials. An orthotropic material is characterized by 9 independent elastic constants:

- 3 Young's moduli (E_{11} , E_{22} , E_{33})
- 3 Poisson's ratios (ν_{12} , ν_{23} , ν_{31})
- 3 shear moduli (G_{12} , G_{23} , G_{31})

Because of the symmetric nature of transversely isotropic materials these constants reduce to 5:

- 2 Young's moduli (E_{11} , E_{22})
- 2 Poisson's ratios (ν_{12} , ν_{23})
- 1 shear moduli (G_{12})

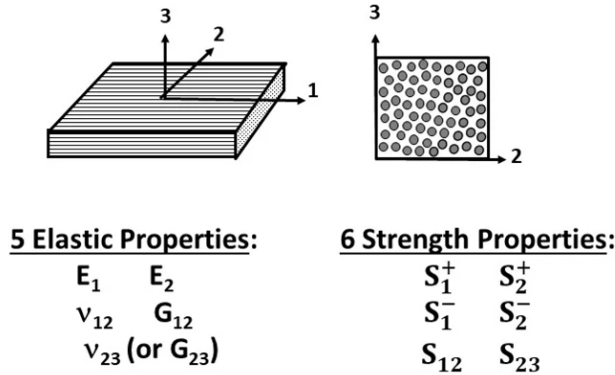


Figure 7. Transversely isotropic material properties

The compliance matrix of a transversely isotropic material, with 23 as the isotropic plane is:

$$\begin{bmatrix} \varepsilon_{11} \\ \varepsilon_{22} \\ \varepsilon_{33} \\ 2\varepsilon_{23} \\ 2\varepsilon_{31} \\ 2\varepsilon_{12} \end{bmatrix} = \begin{bmatrix} 1/E_{11} & -\nu_{21}/E_{22} & -\nu_{21}/E_{22} & 0 & 0 & 0 \\ -\nu_{12}/E_{11} & 1/E_{22} & -\nu_{32}/E_{22} & 0 & 0 & 0 \\ -\nu_{12}/E_{11} & -\nu_{23}/E_{22} & 1/E_{22} & 0 & 0 & 0 \\ 0 & 0 & 0 & 1/G_{23} & 0 & 0 \\ 0 & 0 & 0 & 0 & 1/G_{12} & 0 \\ 0 & 0 & 0 & 0 & 0 & 1/G_{12} \end{bmatrix} \begin{bmatrix} \sigma_{11} \\ \sigma_{22} \\ \sigma_{33} \\ \sigma_{23} \\ \sigma_{31} \\ \sigma_{12} \end{bmatrix}$$

with:

$$G_{23} = \frac{E_{22}}{2(1 + \nu_{23})}, \quad \frac{\nu_{12}}{E_{11}} = \frac{\nu_{21}}{E_{22}}, \quad \nu_{23} = \nu_{32}$$

One notable application of transversely isotropic materials is found in pultruded beams. Pultrusion is a manufacturing process where continuous fibers, such as fiberglass, carbon, or aramid, are impregnated with a polymer resin and pulled through a heated die. This process imparts transverse isotropy to the resulting composite material. The fibers align along the length of the beam, creating a preferred axis that influences the mechanical behavior of the material.

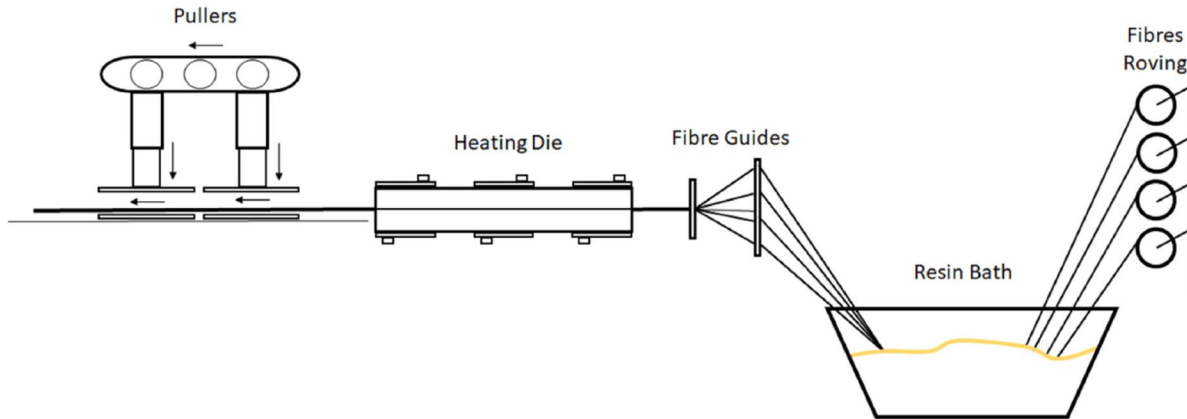


Figure 8. Pultrusion process

In Table 1. are listed the elastic properties of GFRP and CFRP.

Table 1. CFRP & GFRP elastic properties 10

FRP composite (1)	Elastic modulus (GPa) (2)	Major Poisson's ratio (3)	Limiting stress (MPa) (4)	Limiting strain (5)	Shear modulus (GPa) (6)	Thickness of sheet (mm) (7)
Carbon fiber-reinforced polymer (CFRP) laminate	$E_x = 62.0$	$\nu_{xy} = .220$	760	0.012	$G_{xy} = 3.27$	1.0
	$E_y = 4.83$	$\nu_{xz} = .220$			$G_{xz} = 3.27$	
	$E_z = 4.83$	$\nu_{yz} = .300$			$G_{yz} = 1.86^*$	
Glass fiber-reinforced polymer (GFRP) laminate	$E_x = 20.7$	$\nu_{xy} = 0.260$	414	0.02	$G_{xy} = 1.52$	1.3
	$E_y = 6.89$	$\nu_{xz} = 0.260$			$G_{xz} = 1.52$	
	$E_z = 6.89$	$\nu_{yz} = 0.300$			$G_{yz} = 2.65^*$	

* $G_{yz} = (E_y \text{ or } z) / 2(1 + \nu_{yz})$.

2.3 Finite Element Method

The Finite Element Method (FEM) is a powerful numerical technique for solving physical and engineering problems described by differential equations. FEM is useful for problems with complicated geometries, loadings and material properties where analytical solutions cannot be obtained.

A structure is discretized to finite elements connected with each other at the nodes. The displacements of the elements are described by the displacements of the element's nodes with the shape function.

The shape function approximates the behavior of physical quantities (such as displacements, temperatures, etc.) within an element. If we focus on the displacements, the equation below describes the shape function:

$$\mathbf{q}(x, y, z) = \mathbf{N}(x, y, z) \cdot \mathbf{q}^e$$

where:

- $\mathbf{q}(x, y, z)$: the displacements function
- $\mathbf{N}(x, y, z)$: the shape function
- \mathbf{q}^e : the displacement values at the nodes

The strains of the elements are connected with the displacements through the equation:

$$\boldsymbol{\varepsilon} = \mathbf{B} \cdot \mathbf{q}^e$$

where:

$$\mathbf{B} = \boldsymbol{\aleph} \cdot \mathbf{N}(x, y, z), \quad \boldsymbol{\aleph} = \begin{bmatrix} \frac{\partial}{\partial x} & 0 & 0 \\ 0 & \frac{\partial}{\partial y} & 0 \\ 0 & 0 & \frac{\partial}{\partial z} \\ \frac{\partial}{\partial y} & \frac{\partial}{\partial x} & 0 \\ 0 & \frac{\partial}{\partial z} & \frac{\partial}{\partial y} \\ \frac{\partial}{\partial z} & 0 & \frac{\partial}{\partial x} \end{bmatrix}$$

\mathbf{B} is called strain-displacement matrix and $\boldsymbol{\aleph}$ is an operator matrix.

The stresses of the elements are connected with the strains through the elastic constants matrix:

$$\boldsymbol{\sigma} = \mathbf{D} \cdot \boldsymbol{\varepsilon}$$

\mathbf{D} is the inverse of the compliance matrix and is also called stiffness matrix (not to be confused with the stiffness matrix \mathbf{K} defined in the FEM).

D depends on the type of the material (isotropic, orthotropic, etc.) and the type of the problem (plain stress, plain strain, etc.)

The forces acting on an element's nodes are connected to the displacements with the element's stiffness matrix:

$$\mathbf{F}^e = \mathbf{k}^e \cdot \mathbf{q}^e$$

where:

$$\mathbf{k}^e = \int_{V^e} \mathbf{B}^T \mathbf{D} \mathbf{B} \cdot dV$$

If the problem is static, by combining the force-displacement equations of all the nodes we get the system:

$$\mathbf{R} = \mathbf{K} \cdot \mathbf{r}$$

where:

- \mathbf{R} : the structure force vector
- \mathbf{r} : the structure displacement vector
- \mathbf{K} : the structure stiffness matrix

If the problem is a linear instability problem, like linear buckling, the system of equations takes the form:

$$\mathbf{R} = (\mathbf{K} + \mathbf{K}_o) \cdot \mathbf{r}$$

where:

- \mathbf{K}_o : the geometric stiffness matrix

\mathbf{K}_o is proportional to an initial constant axial or membrane load and is derived by taking into account the higher order terms that are discarded on the small displacement theory. The geometry stiffness matrix can be written to the form:

$$\mathbf{K}_o = \lambda \mathbf{K}_o^*$$

where \mathbf{K}_o^* is the geometry stiffness matrix created by a unit load and λ a multiplier.

To calculate the critical load we have to solve for λ :

$$\det(\mathbf{K} + \lambda \mathbf{K}_o^*) = \mathbf{0}$$

The equation has a number of solutions, depending on the discretization of the structure, λ_i ($i = 1, 2, \dots, n$). From the above, only λ_{\min} has actual physical meaning because it is the minimum critical load on which the structure becomes unstable.

2.3.1 Shell elements

In structural analysis of thin plates, three dimensional shell elements with 6 degrees of freedom per node (3 translational and 3 rotational) are used to model complex behaviors like bending and buckling of plates.

The most common shell elements in commercial FEA programs like ABAQUS and ANSYS are the universal serendipity elements (USE) defined as isoparametric elements with corner and mid-edge nodes only.

The 1st order shell element is a quadrilateral with 4 nodes, 1 at each corner, and it belongs to the Lagrange family of isoparametric elements. The quadratic and cubic USEs differ from the Lagrange because they are missing the mid-surface nodes.

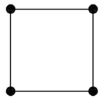
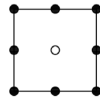
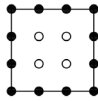
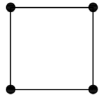
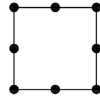
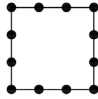
	Linear	Quadratic	Cubic
Lagrange			
Serendipity			

Figure 9. Shell elements sorted by their nodes

Triangular elements can also be used instead of quadrilateral but show some serious disadvantages (like numerical instability, shear locking, low interpolation accuracy, etc.) that make them unsuitable to produce accurate results.

The ABAQUS quadrilateral shell elements used for structural analysis are:

- S4R: linear 4-node reduced integration shell element
- S8R: quadratic 8-node reduced integration shell element

both elements belong to the USE family and use reduced integration.

The integration above refers to the number of integration points used in the Gauss-Lagrange numerical integration that takes place when calculating the element stiffness matrix \mathbf{k}^e . When the number of integration points is less than the required number to get a result equal to the analytical solution, the element is characterized with reduced integration.

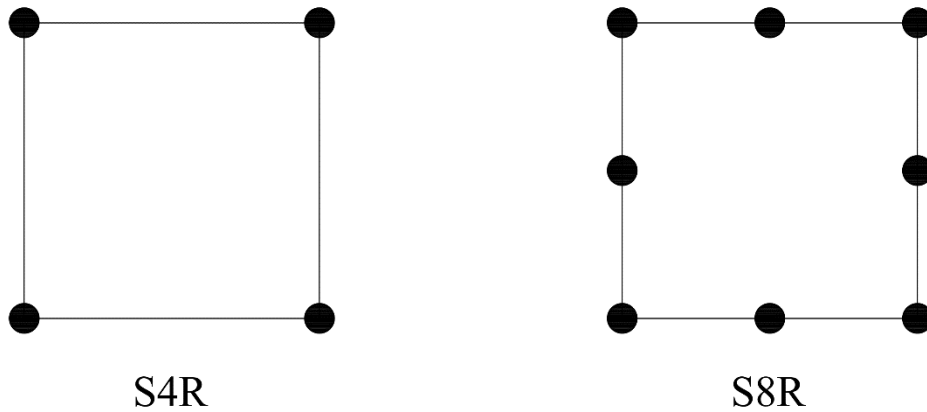


Figure 10. ABAQUS quadrilateral shell elements

2.4 Statistical Analysis

2.4.1 Central Limit Theorem

Central Limit Theorem (CLT) is a fundamental concept in probability theory and statistics. It states that if X_1, X_2, \dots, X_n is a random sample of size n taken from a population with mean μ and finite variance σ^2 and if \bar{X} is the sample mean, the limiting form of the distribution of:

$$Z = \frac{\bar{X} - \mu}{\sigma/\sqrt{n}}$$

as $n \rightarrow \infty$, is the standard normal distribution $N(0,1)$. [8]

2.4.2 Confidence intervals

A confidence interval (CI) estimate for μ is an interval of the form $l \leq \mu \leq u$ where the end points are computed from the sample data. Setting l, u to be random variables L, U the following statement is true

$$P(L \leq \mu \leq U) = 1 - a, \quad 0 \leq a \leq 1$$

which means that there is a probability $1 - a$ that the CI $[L, U]$ will contain μ . [8]

Population variance known

If \bar{X} is the sample mean of a large random sample of size n that follows the normal distribution, the CI can be extracted from the central limit theorem as:

$$P\left(\bar{X} - z_{a/2} \frac{\sigma}{\sqrt{n}} \leq \mu \leq \bar{X} + z_{a/2} \frac{\sigma}{\sqrt{n}}\right) = 1 - a$$

where $z_{a/2}$ is the upper $100 a/2$ percentage point of the standard normal distribution.

In some cases one-sided confidence bounds are used:

A $(100-a)\%$ upper-confidence bound for μ is

$$\mu \leq \bar{X} + z_a \frac{\sigma}{\sqrt{n}}$$

A $(100-a)\%$ lower-confidence bound for μ is

$$\bar{X} - z_a \frac{\sigma}{\sqrt{n}} \leq \mu$$

where z_a is the upper $100a$ percentage point of the standard normal distribution. [8]

Population variance unknown

For the general case where the variance is unknown and the sample is small, the bounds can be calculated using Student's T distribution.

If \bar{X} is the sample mean of a random sample of size n that follows the normal distribution, the CI can be calculated from:

$$P\left(\bar{X} - t_{a/2}(n) \frac{S}{\sqrt{n}} \leq \mu \leq \bar{X} + t_{a/2}(n) \frac{S}{\sqrt{n}}\right) = 1 - a$$

where $t_{a/2}(n)$ is the upper $100 a/2$ percentage point of the Student's T distribution with n degrees of freedom and S^2 is the sample variance.

Same with one-sided confidence bounds:

A $(100-a)\%$ upper-confidence bound for μ is

$$\mu \leq \bar{X} + t_a(n) \frac{S}{\sqrt{n}}$$

A $(100-a)\%$ lower-confidence bound for μ is

$$\bar{X} - t_a(n) \frac{S}{\sqrt{n}} \leq \mu$$

where $t_a(n)$ is the upper $100a$ percentage point of the Student's T distribution with n degrees of freedom.

As $n \rightarrow \infty$, Student's T distribution converges to the standard normal distribution. [8]

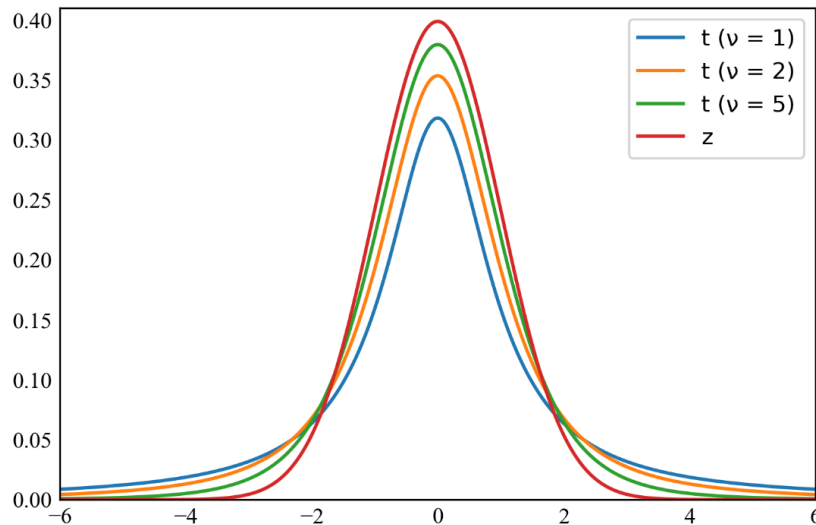
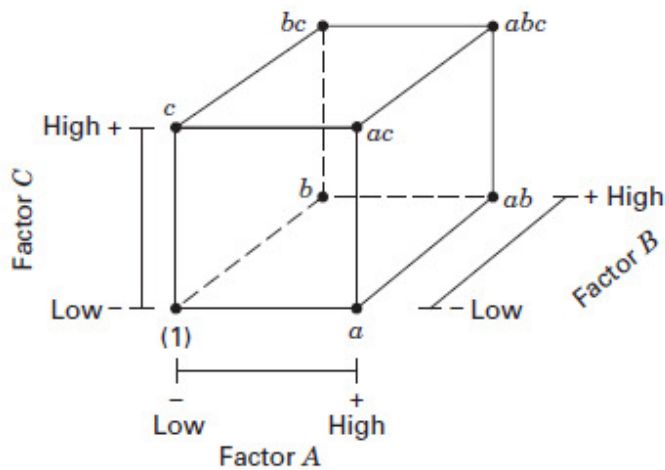


Figure 11. Student's T distribution for various degrees of freedom

2.4.3 Factorial design

Factorial design in Design of Experiments (DoE) is a method that examines the effects a number of independent variables (factors) has to a dependent variable of interest. They are the most efficient designs for experiments that include two or more factors. By factorial it is meant that every possible combination of the factors at each level is taken into consideration. The levels may be quantitative, such as values of temperature, or they may be qualitative, such as different machines.



(a) Geometric view

Run	Factor		
	A	B	C
1	-	-	-
2	+	-	-
3	-	+	-
4	+	+	-
5	-	-	+
6	+	-	+
7	-	+	+
8	+	+	+

(b) Design matrix

Figure 12. 2³ Factorial example

A widely used type of factorial design is the 2^k factorial design because it forms the basis of other designs of considerable practical value. It suggests that by having k factors, you only consider the “low” and the “high” levels of the factors. Each factor has two levels, so the number of all the possible combinations is $2 \times 2 \times \dots \times 2 = 2^k$ as the name states. If, instead of low and high levels, a middle level is included to the factors of a 2^k design, the design becomes 3^k factorial. These types of design are useful for examining the effects and the interaction of the factors.

Factorial design is the first step of an experimental process, it helps distinguish the significant factors from the insignificant ones in order to proceed to more practical methods to extract results that can be utilized. [9]

2.4.4 Response surface methodology

Response Surface Methodology (RSM), like factorial design, is a statistical technique used in experimental design. Unlike factorial design, RSM emphasizes the optimization of a response variable by fitting a response surface to a set of experimental data. The experimental data can be the response values at the factor levels of a factorial design.

If the observed response y is of the form:

$$y = f(x_1, x_2, \dots, x_n) + \epsilon$$

where ϵ is the noise of the observed response and x_1, x_2, \dots, x_n are the factors, the surface represented by:

$$\eta = f(x_1, x_2, \dots, x_n)$$

is called a response surface.

If the problem examined can be reduced to two factors, the response surface is a 3-dimensional surface that can be visualized through contour plots in order to extract useful data for optimization processes etc.

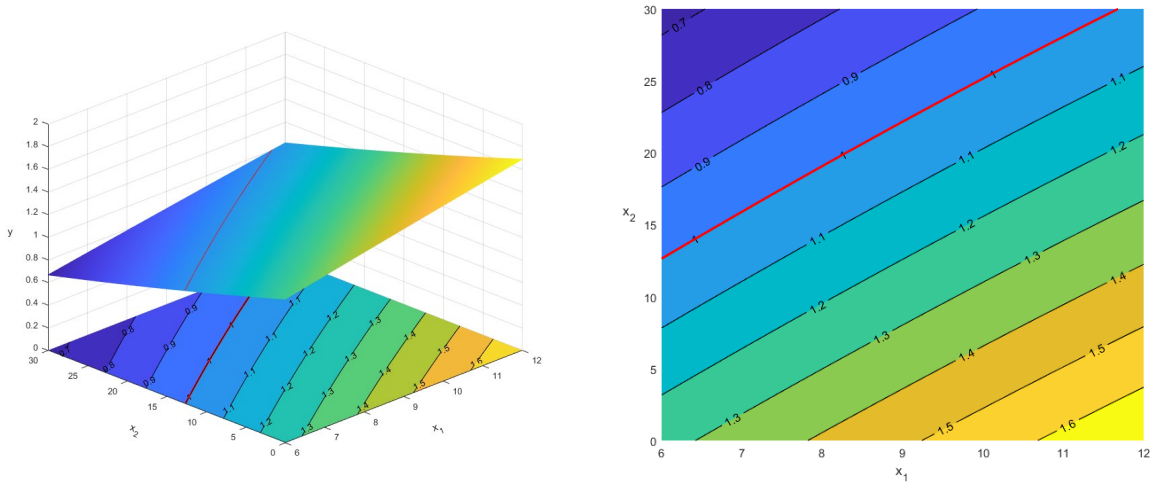


Figure 13. Response surface example

Although RSM is commonly used for optimization processes, like finding the minimum or the maximum of a response, it can also be used to extract useful formulas and contours that can be used for reverse engineering. For example let's assume a repair problem, the factor x_2 is measured to be 20 and the response y should be greater than 1 in order to have an acceptable design, by using the contour in the figure XX, the factor x_1 must be greater than 8.5. The bigger x_1 becomes the bigger the repair cost, so by choosing $x_1 = 9$ the result of the design is optimal. [9]

2.4.5 Central composite design

Central Composite Design (CCD) is a method used for the selection of the points that will be interpolated by the response surface. A CCD consists of the factorial points, the axial points and the center points. The location of the axial points characterize the type of CCD, as shown in figure. The low level is symbolized with -1 and the high level with +1. The value of α is calculated from the formula:

$$\alpha = [2^k]^{1/4}$$

Circumscribed [CCC]	Face Centered [CCF]	Inscribed [CCI]

Figure 14. CCD types

There are three types of CCD:

- Circumscribed (CCC)
- Face-centered (CCF)
- Inscribed (CCI)

Both the CCC and CCI are rotatable designs, which means that the variance of the predicted response at points with equal distance from the center is the same. CCF is not rotatable but it is used when the region of interest is cuboidal and not spherical. The points of a CCF are the points of a 3^k factorial design.

RSM combined with CCD produce a robust model that can be used to describe a big variety of experimental analyses. CCD enables the points to fit to a 2nd order polynomial RSM of the form:

$$\eta = \beta_0 + \sum_i \beta_i x_i + \sum_i \beta_{ii} x_i^2 + \sum_{j < i} \sum_i \beta_{ij} x_i x_j$$

For an experiment with 2 factors, the response surface is of the form:

$$\eta = \beta_0 + \beta_1 x_1 + \beta_2 x_2 + \beta_{11} x_1^2 + \beta_{22} x_2^2 + \beta_{12} x_1 x_2$$

The surface is fitted to the points through the method of least squares. [9]

3 Geometry and Simulation

A plate with aspect ratio between 1 and $\sqrt{2}$ was chosen to examine how the first modes in bi-axial compression and pure shear react to composite beam reinforcement.

Table 2. Steel plate properties

Property	Symbol	Value	Unit
Material	-	Grade 'A' Steel	-
Length	a	2500	mm
Width	b	1845	mm
Initial thickness	t	17	mm
Young's modulus	E	210	GPa
Poisson's ratio	ν	0.3	-

The plate is end-to-end reinforced (-10 mm at each end) with a number of equally spaced FRP stiffeners. The reinforcement arrangement parameters are shown in Table 3.

Table 3. Reinforcement arrangement parameters

Factor	Details	Levels
A	Stiffener orientation	Parallel or perpendicular to the plate's long side
B	Reinforcement type	Single or double sided
C	Number of stiffeners	1 to 4 per side
D	Stiffener material	GFRP or CFRP
E	Stiffener geometry	Profile, web height, thickness etc.

The selected stiffener is a pultruded T-beam, its properties are shown in Table 4.

Table 4. Composite T-beam properties

Property	Symbol	Value	Unit
Material	-	GFRP	-
Length	L	a – 20	mm
Web height	A	100	mm
Flange width	B	150	mm
Thickness	T	9.5	mm

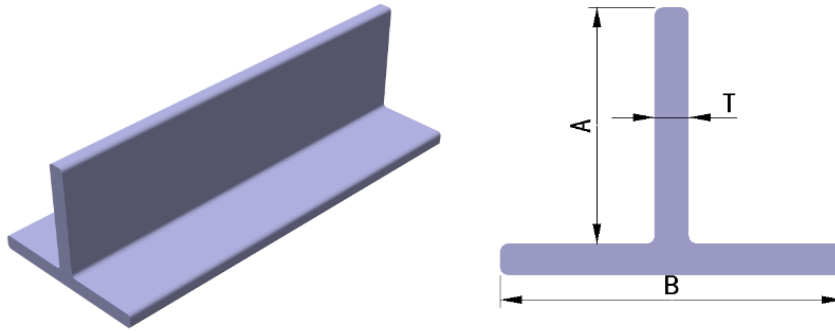


Figure 15. T-beam profile and scantlings

Each simulation extracts a point which is then assigned to a curve $\sigma^*/\sigma - t^*/t$ where:

- σ^* : the critical stress after reinforcement with thickness $t - t^*$
- σ : the critical stress before reinforcement with thickness t
- t : the initial thickness
- t^* : the lost thickness due to uniform corrosion (0-6 mm)

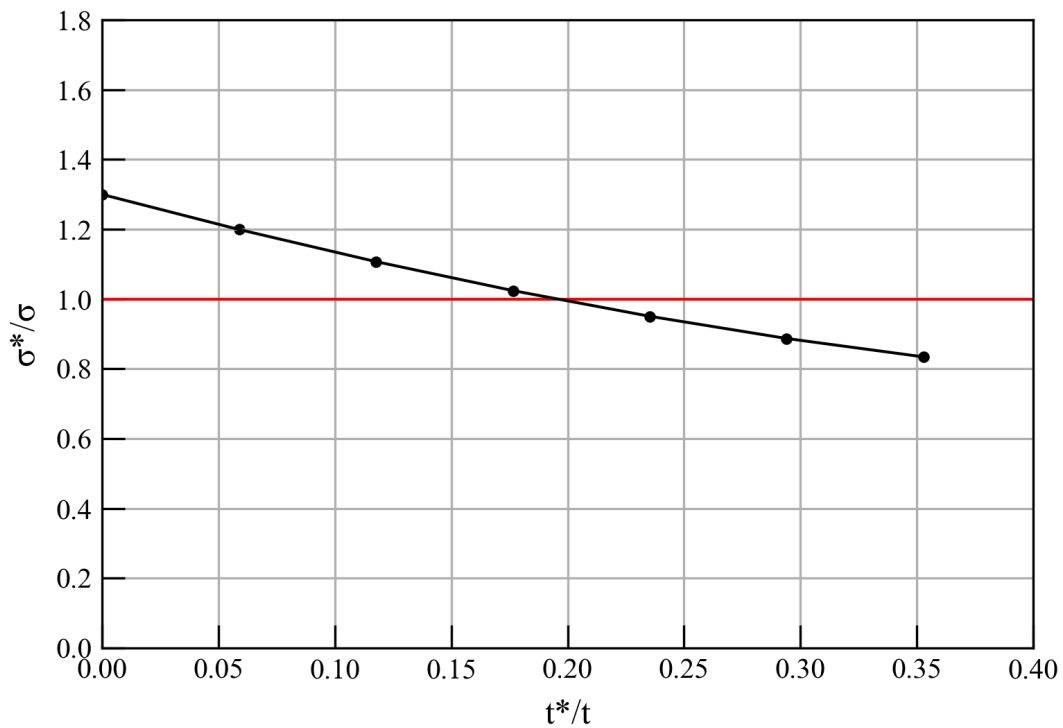


Figure 16. $\sigma^*/\sigma - t^*/t$ curve example

3.1 FEM Modeling

The simulations were programmed using the general-purpose FEA software Abaqus/CAE.

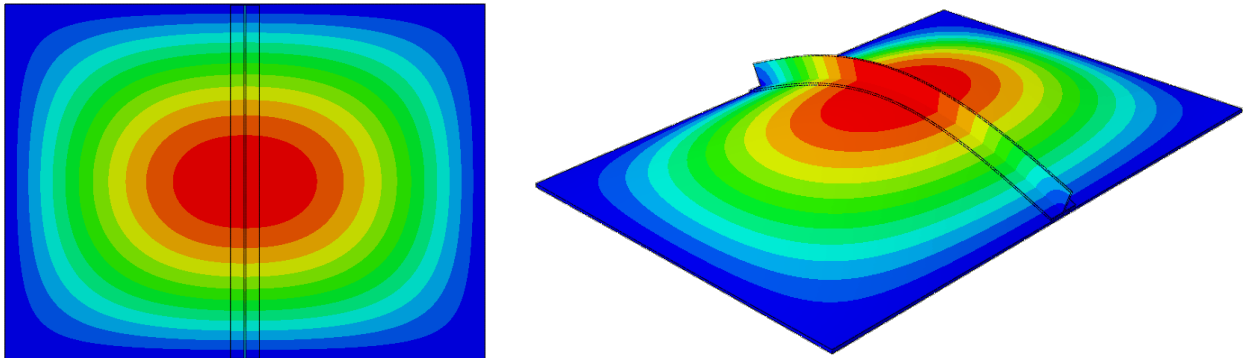


Figure 17. Reinforced plate in bi-axial compression

The first stage of the modeling is to import the elastic material properties for steel and FRPs. Steel is imported as an isotropic material with E and ν as its only constants. FRP is imported with the option of Engineering Constants which are the 9 elastic constants that characterize an orthotropic material (Section 2.2).

3.1.1 Steel plate

The steel plate is modeled as a 3D deformable planar shell. Then a section is assigned to it with the geometric (constant thickness) and material (isotropic E, ν) properties. The plate is then meshed with rectangular elements and assigned element types.

3.1.2 FRP flange

The FRP flange is implemented as an instance in the steel plate. A composite layup of conventional shell elements is added to replace the steel plate section. Depending on the type of reinforcement, single or double sided, the composite layups modeling is different.

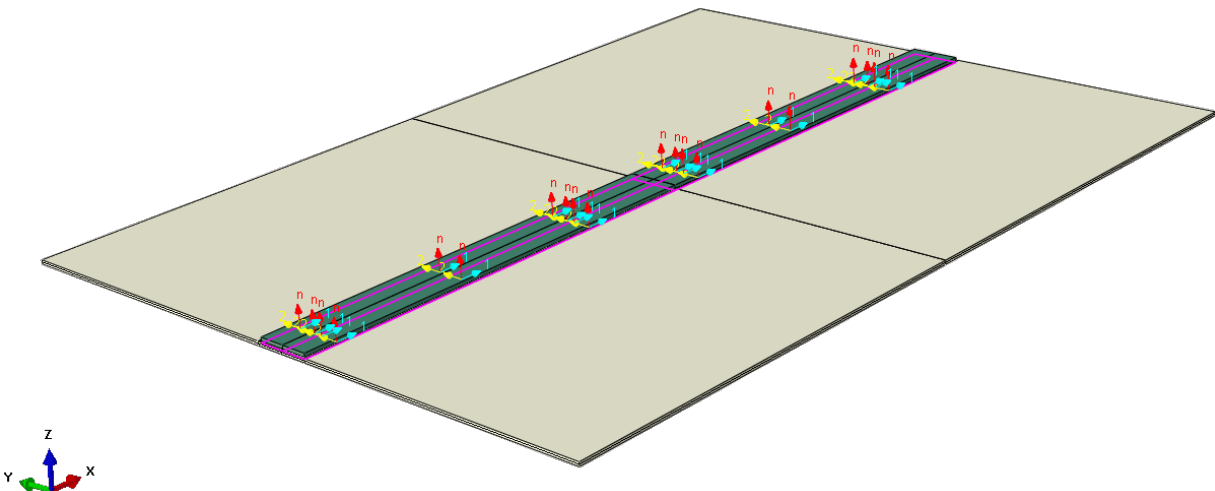


Figure 18. Composite flange fiber orientation

Single-sided reinforcement



Figure 19. Single-sided reinforcement section

The layup consists of 2 plies. The first ply has steel section with thickness equal to the plates and the second ply has FRP section with the stiffener's thickness. The fibers' orientation is parallel to the stiffeners longitudinal axis. The layup's mid-plane must be shifted downwards to align the steel sections, this is achieved with the offset option. The offset is calculated with the formula:

$$offset\ ratio = \pm 0.5 \cdot \left[1 - \frac{t_{steel}}{t_{steel} + t_{FRP}} \right]$$

The sign depends on the side of the plate the stiffener is placed.

Double-sided reinforcement



Figure 20. Double sided reinforcement section

The layup consists of 3 plies. The first ply has FRP section with the stiffener's thickness, the second ply has steel section with the plate's thickness and the third ply is the same as the first. The offset in this case is zero due to the symmetry.

3.1.3 FRP web

The FRP web is modeled as a 3D deformable planar shell, like the steel plate. Its section is a 1-ply composite layup. The fibers' orientation is parallel to the stiffeners longitudinal axis. The web is connected to the flange with a Tie constraint, with primary surface the middle of the flange instance and secondary the web's edge.

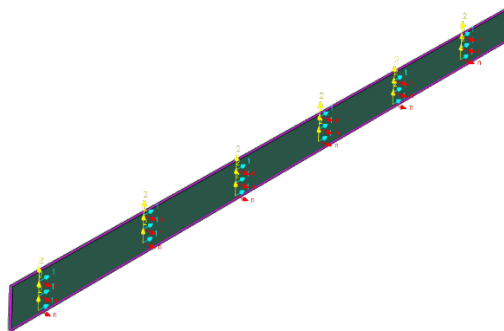


Figure 21. Composite web fiber orientation

The web height should also have offset equal to:

$$d = t_{plate}/2 + t_{flange}$$

from the mid-plane because part of it intersects the plate and the flange and the total height is not being utilized in the simulation. The suggested way to deal with this problem, since there is no solution for this in the program, is to increase the web's height. Having as a constant the 2nd moment of area of the web around the mid-plane, the new height is calculated:

$$I_{XX} = \frac{t \cdot h^3}{12} + t \cdot h \cdot \left(\frac{h}{2} + d\right)^2 = \frac{th^3}{3} + t \cdot d \cdot h^2 + t \cdot d^2 \cdot h$$

$$I_{XX}^* = \frac{t \cdot h^{*3}}{12} + t \cdot h^* \cdot \left(\frac{h^*}{2}\right)^2 = \frac{t \cdot h^{*3}}{3}$$

$$I_{XX} = I_{XX}^* \rightarrow \frac{h^*}{h} = \left(1 + 3 \left[\left(\frac{d}{h}\right) + \left(\frac{d}{h}\right)^2 \right]\right)^{\frac{1}{3}} \approx 1 + \frac{d}{h}, \quad \text{for } \frac{d}{h} \ll 1$$

It is proven that the corrected web height is:

$$h^* \approx h + d$$

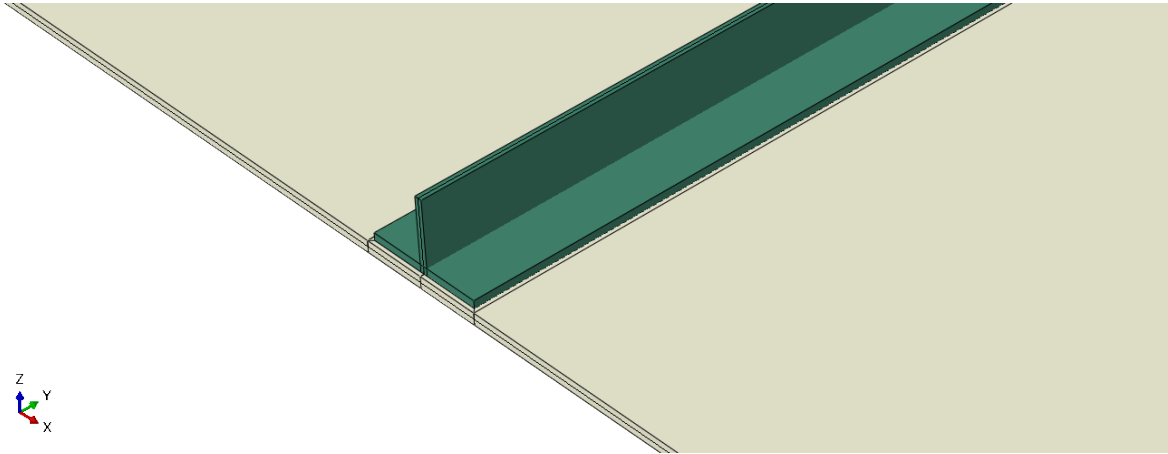


Figure 22. Composite T-beam result

3.1.4 Steps

The analysis steps consist of the initial step, in which the boundary conditions are implied, and the final step, which is a linear buckle step. In the buckle step the loads are applied to the reference points (RP-i) as unit forces with units [N]. The reference points are connected to the plate with coupling constraints.

Using this method instead of applying an edge load makes possible the use of the same model for displacement controlled non-linear analysis.

3.1.5 Loads, BCs and constraints

The loads, boundary conditions and constraints used for the model are different for the bi-axial compression model and the pure shear model.

Bi-axial compression

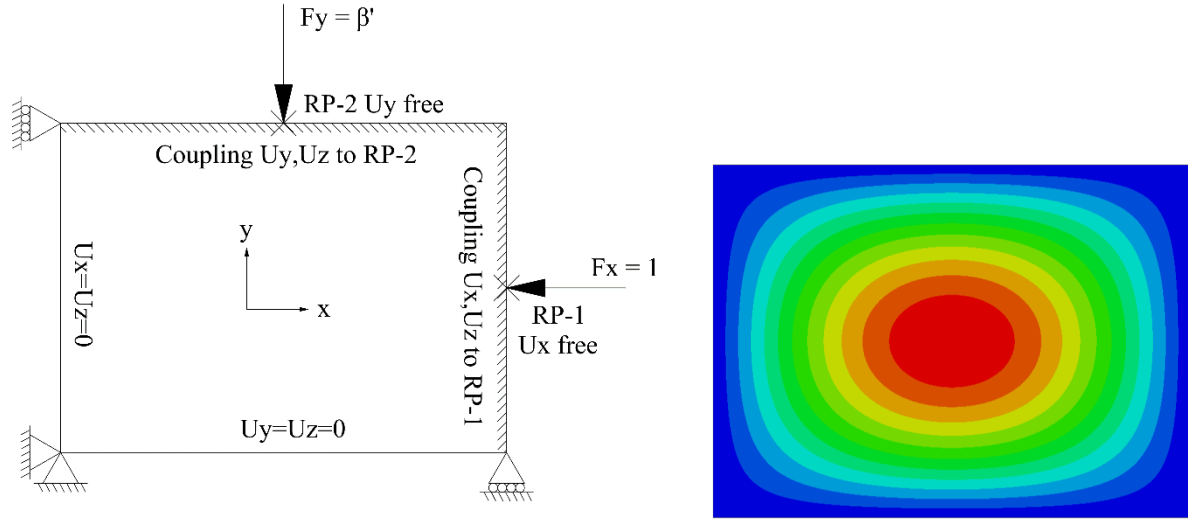


Figure 23. Bi-axial compression loads and boundary conditions

The boundary conditions are simple-support. All the edges are free to rotate and not permitted to move out-of-plane ($U_z = 0$).

The only degree of freedom (DoF) RP-1 has is translation along the x-axis. RP-1 is coupled with the plate's edge for the U_x and U_z DoFs. The analogous applies for RP-2 along the y-axis.

The load F_x applied to RP-1 simulates the N_x and the load F_y applied to RP-2 the N_y . In bi-axial compression the formula below must be satisfied:

$$\beta = \frac{N_y}{N_x}$$

But the loads applied to the plate are forces, so:

$$N_y = \frac{F_y}{a}, \quad N_x = \frac{F_x}{b} \rightarrow \beta = \frac{F_y}{F_x} \cdot \frac{b}{a} = \frac{F_y}{F_x} \cdot \frac{1}{r}$$

The following must be true for the forces:

$$\beta' = \frac{F_y}{F_x}, \quad \beta' = \beta \cdot r$$

Meaning, by setting $F_x = 1$ then $F_y = \beta'$.

Pure shear

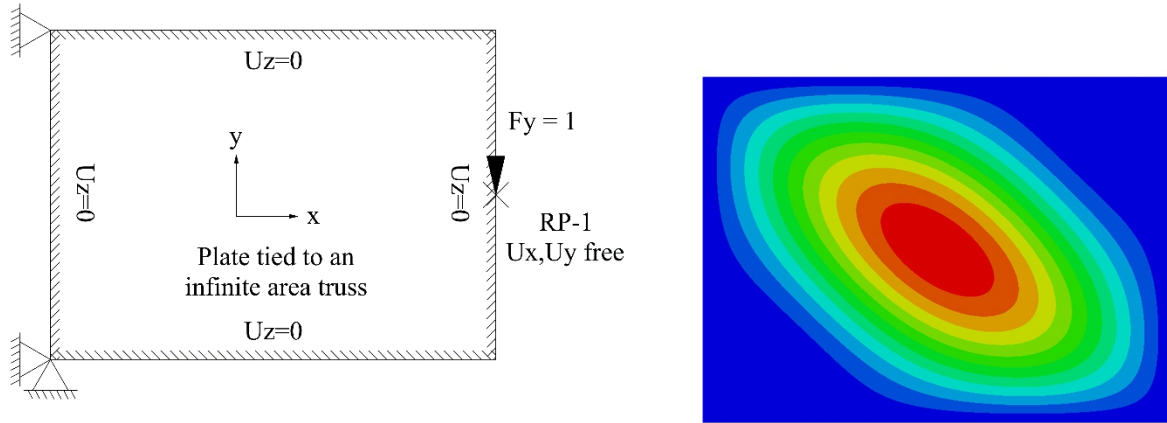


Figure 24. Pure shear boundary conditions and loads

The boundary conditions are simple-support (hinged). The effects of pure shear stresses on an infinitely small element is the change of its angle while the edges form and length stay undisturbed (shear strain).

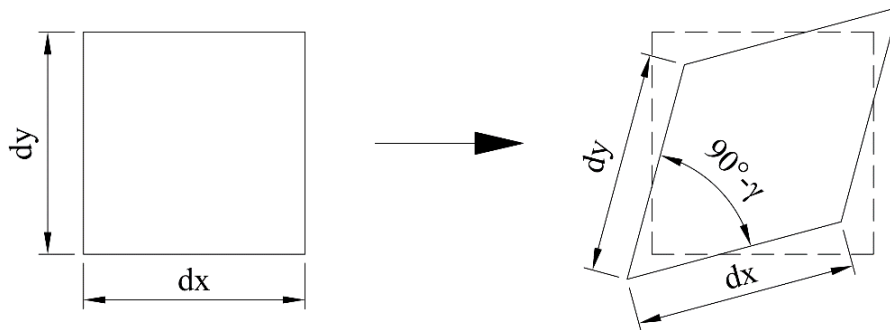


Figure 25. Pure shear in infinitely small element

The opposite can also be said because of the linear relationship of shear stress (τ) and shear strain (γ) given by the formula of the shear modulus:

$$\tau = G \cdot \gamma \leftrightarrow \gamma = \frac{1}{G} \cdot \tau$$

By integrating this concept for a plate of dimensions $a \times b$, if the plates edges are forced to stay intact while the angle γ increases, the plate will be subjected to pure shear. A way to achieve it is with the use of an auxiliary mechanism, a rectangular truss of dimensions $a \times b$ that consist of rigid rods free to rotate at the nodal point. By coupling the plate's translational DoFs at the edges to the truss while letting the rotational DoFs free simple-support conditions are achieved.

The load F_y is applied to RP-1. RP-1 is coupled to the truss and free to move at the xy plane.

3.1.6 Post-processing

Bi-axial compression

The extracted data from a simulation is an eigenvalue in force units [N]. This value inserted to a formula to get the critical buckling stress:

$$\sigma_x^* [MPa] = f(F_x, b, t, t^*) = \frac{F_x}{b \cdot (t - t^*)}$$

where:

- $F_x [N]$: FEA eigenvalue
- $b [mm]$: breadth of the edge
- $t [mm]$: initial plate thickness
- $t^* [mm]$: thickness reduction due to corrosion

The stress of the other edge is calculated with the formula:

$$\sigma_y^* = \beta \cdot \sigma_x^*$$

Pure shear

The extracted data from a simulation is an eigenvalue in force units [N]. This value inserted to a formula to get the critical buckling stress:

$$\tau^* [MPa] = f(F_y, b, t, t^*) = \frac{F_y}{b \cdot (t - t^*)}$$

where:

- $F_y [N]$: FEA eigenvalue
- $b [mm]$: breadth of the edge
- $t [mm]$: initial plate thickness
- $t^* [mm]$: thickness reduction due to corrosion

4 Numerical Results

In this section are presented the numerical results of the FEA simulations.

4.1 Model verification

The bi-axial compression and the pure shear models were tested for both static linear perturbation analysis and buckling analysis for a steel plate. The results were then compared with theoretical formulas.

Bi-axial compression

A static analysis was ran with $F_x = 10^6$ N, $\beta = 0.5$, $F_y = \beta \cdot F_x = 0.678 \cdot 10^6$.

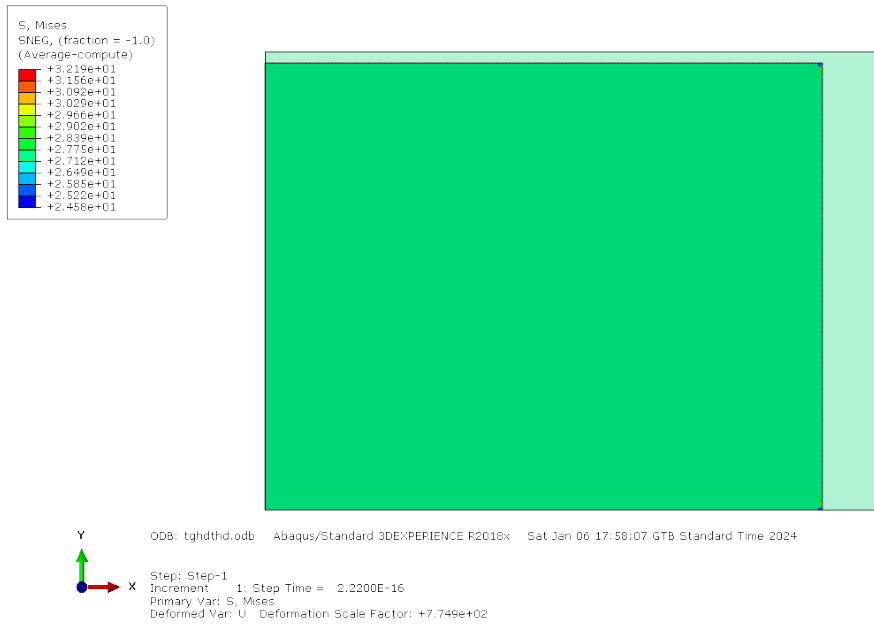


Figure 26. Plate in bi-axial compression in static FEA model

The theoretical results for the uniform stresses are:

$$\sigma_x = \frac{F_x}{A} = \frac{F_x}{b \cdot t} = \frac{-10^6}{1845 \cdot 17} = -31.883 \text{ MPa}, \quad \sigma_y = \beta \cdot \sigma_x = -15.941 \text{ MPa}$$

$$\sigma_{Mises} = \sqrt{\sigma_x^2 + \sigma_y^2 - \sigma_x \cdot \sigma_y} = 27.611 \text{ MPa}$$

The experimental results that were extracted from the bi-axial compression model are:

$$\sigma_{x,FEA} = -31.883 \text{ MPa}, \quad \sigma_{y,FEA} = -15.941 \text{ MPa}, \quad \sigma_{Mises,FEA} = 27.611 \text{ MPa}$$

A buckle analysis was ran with $F_x = 1$, $\beta = 0.5$, $F_y = \beta' = 0.678$.

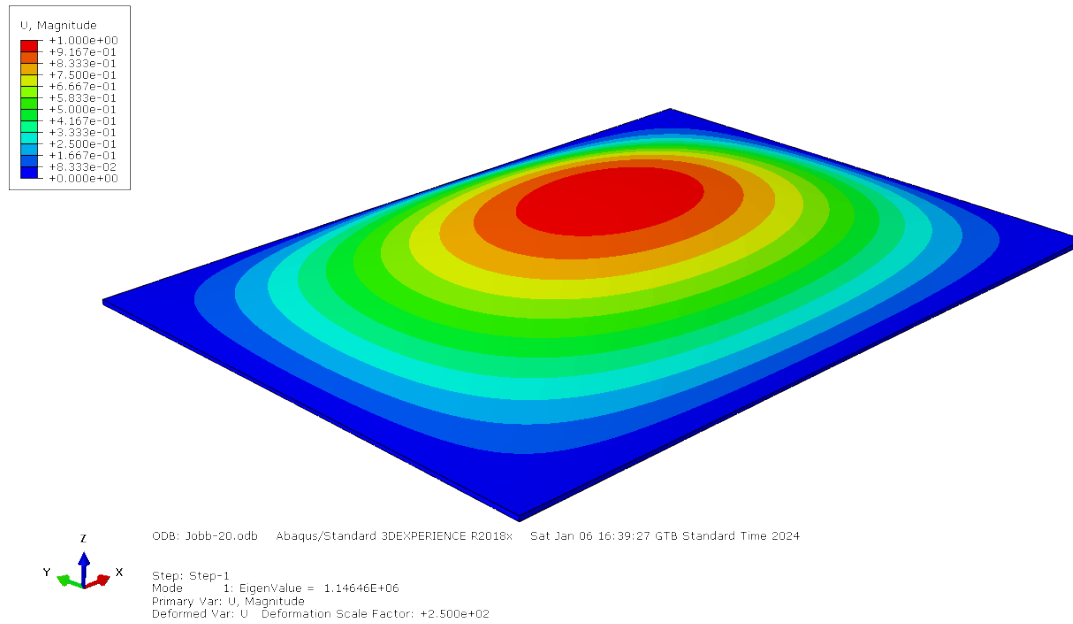


Figure 27. Plate in bi-axial compression in buckle FEA model

The theoretical result for the critical buckling stress is:

$$\sigma_x = K_C \cdot \frac{D\pi^2}{b^2t} = 36.804 \text{ MPa}, \quad K_C = \left[\frac{1}{r} + r \right]^2 \frac{1}{1 + \beta r^2} = 2.284$$

The experimental result that was extracted from the bi-axial compression model is:

$$F_x = 1146460 \text{ N}$$

In stress units:

$$\sigma_{x,FEA} = \frac{F_x}{b \cdot t} = 36.552 \text{ MPa}$$

Pure shear

A static analysis was ran with $F_y = 10^6$ N.

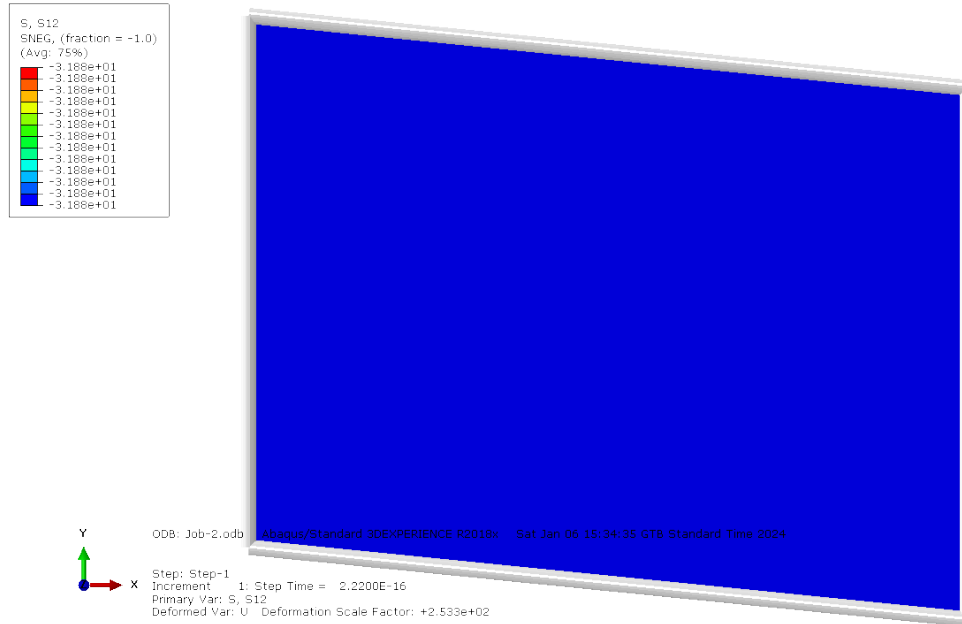


Figure 28. Plate in pure shear in static FEA model

The theoretical result for the uniform shear stress is:

$$\tau = \frac{F}{A} = \frac{F}{b \cdot t} = \frac{10^6}{1845 \cdot 17} = 31.883 \text{ MPa}$$

The experimental result that was extracted from the pure shear model is:

$$\tau_{FEA} = 31.883 \text{ MPa}$$

The normal stresses have magnitude equal to 10^{-12} MPa which is considered to be computational noise.

A buckle analysis was ran with $F_y = 1$.

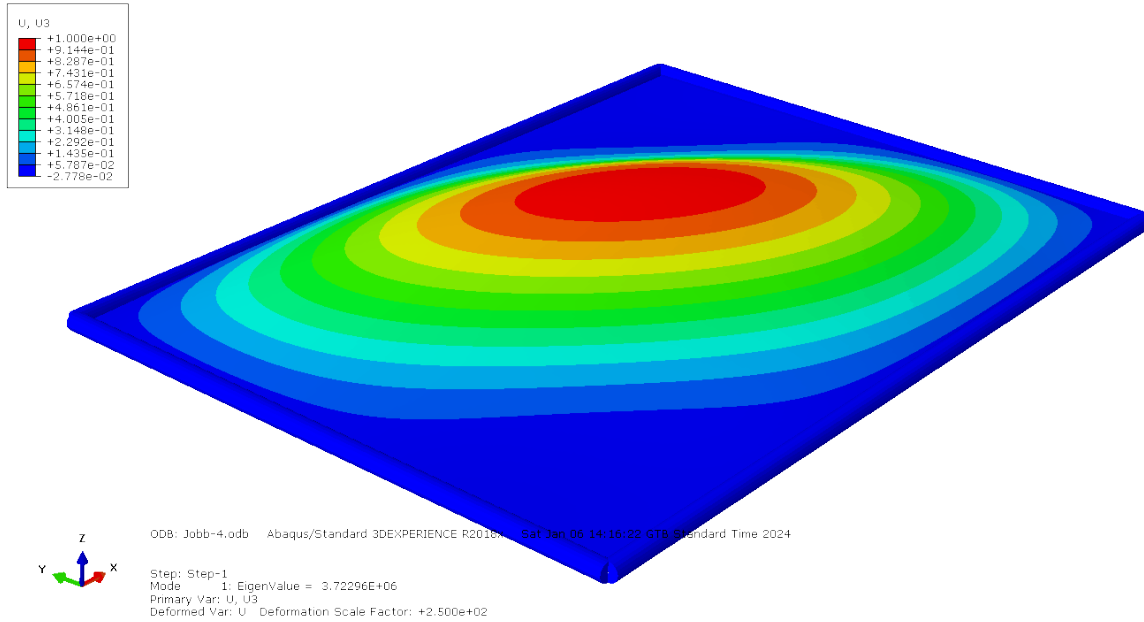


Figure 29. Plate in pure shear in buckle FEA model

The theoretical result for the critical buckling shear stress is:

$$\tau = K_S \cdot \frac{D\pi^2}{b^2t} = 118.819 \text{ MPa}, \quad K_S = 7.374 \text{ (Fig. xx)}$$

The experimental result that was extracted from the pure shear model is:

$$F_y = 3722960 \text{ N}$$

In stress units:

$$\tau_{FEA} = \frac{F_y}{b \cdot t} = 118.698 \text{ MPa}$$

The edges are free to rotate confirming that simple-support conditions are in order.

4.2 Simulations results

Each graph has a title of the form:

"XXXX YZ"

where:

- XXXX: the type of load
- Y=[T/L]: the orientation of the stiffeners
 - T: Transverse or perpendicular to the plate's long side
 - L: Longitudinal or parallel to the plate's long side
- Z=[S/D]: the type of reinforcement
 - S: single-sided reinforcement
 - D: double-sided reinforcement

The $n = 0,1,2,3,4$ at the end of each curve is the number of stiffeners per side, with 0 being the unreinforced plate which was added to each graph for reference. The red line is the baseline of the repair design, if a point is above it, its critical buckling value exceeds the critical buckling value of the uncorroded plate.

For the case of bi-axial compression, only the sub-cases of uni-axial compression in both axes ($\beta = 0.0 / \beta = \infty$) and equi-bi-axial compression ($\beta = 1.0$) were examined. After concluding that longitudinal reinforcement was superior and more stable on average, more simulations were run for it for the case of bi-axial compression for values of β equal to: [0.2, 0.4, 0.6, 0.8, 1:0.8, 1:0.6, 1:0.4, 1:0.2]. Their results showed great similarities with the sub-case of equi-bi-axial compression, and were presented combined to a graph showing their average, min and max values.

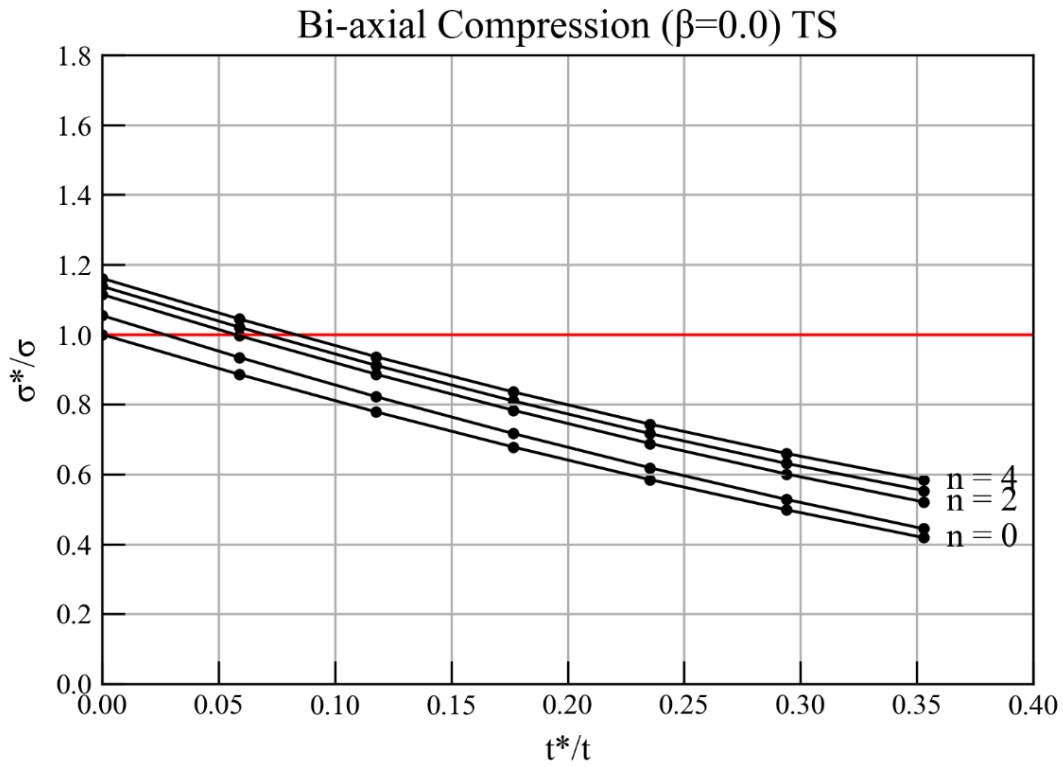


Figure 30. Reinforcement case: Bi-axial Compression ($\beta=0.0$) TS

Table 5. σ^*/σ values of reinforcement case: Bi-axial Compression ($\beta=0.0$) TS

t^*	$n = 1$	$n = 2$	$n = 3$	$n = 4$
0	1.054	1.114	1.138	1.161
1	0.935	0.997	1.021	1.044
2	0.822	0.886	0.912	0.936
3	0.717	0.784	0.810	0.836
4	0.619	0.688	0.716	0.743
5	0.528	0.601	0.631	0.659
6	0.444	0.521	0.553	0.584

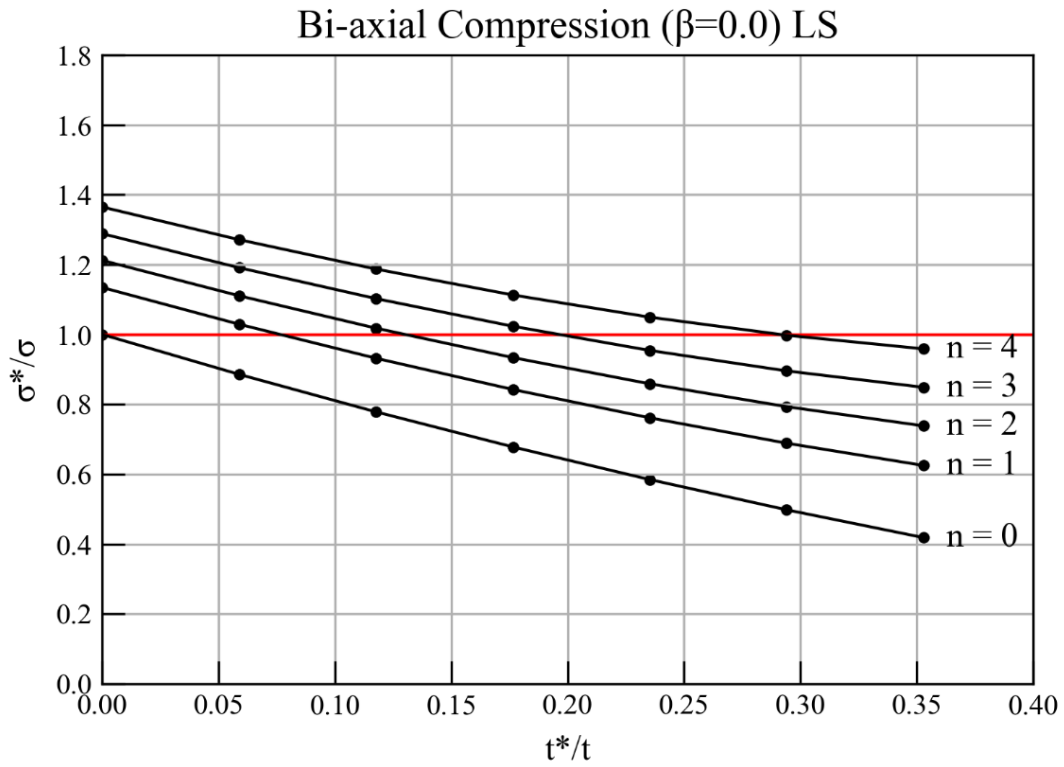


Figure 31. Reinforcement case: Bi-axial Compression ($\beta=0.0$) LS

Table 6. σ^*/σ values of reinforcement case: Bi-axial Compression ($\beta=0.0$) LS

t^*	$n = 1$	$n = 2$	$n = 3$	$n = 4$
0	1.134	1.212	1.288	1.365
1	1.029	1.111	1.191	1.271
2	0.932	1.018	1.103	1.187
3	0.843	0.934	1.024	1.113
4	0.761	0.859	0.954	1.050
5	0.689	0.793	0.896	0.998
6	0.625	0.738	0.849	0.959

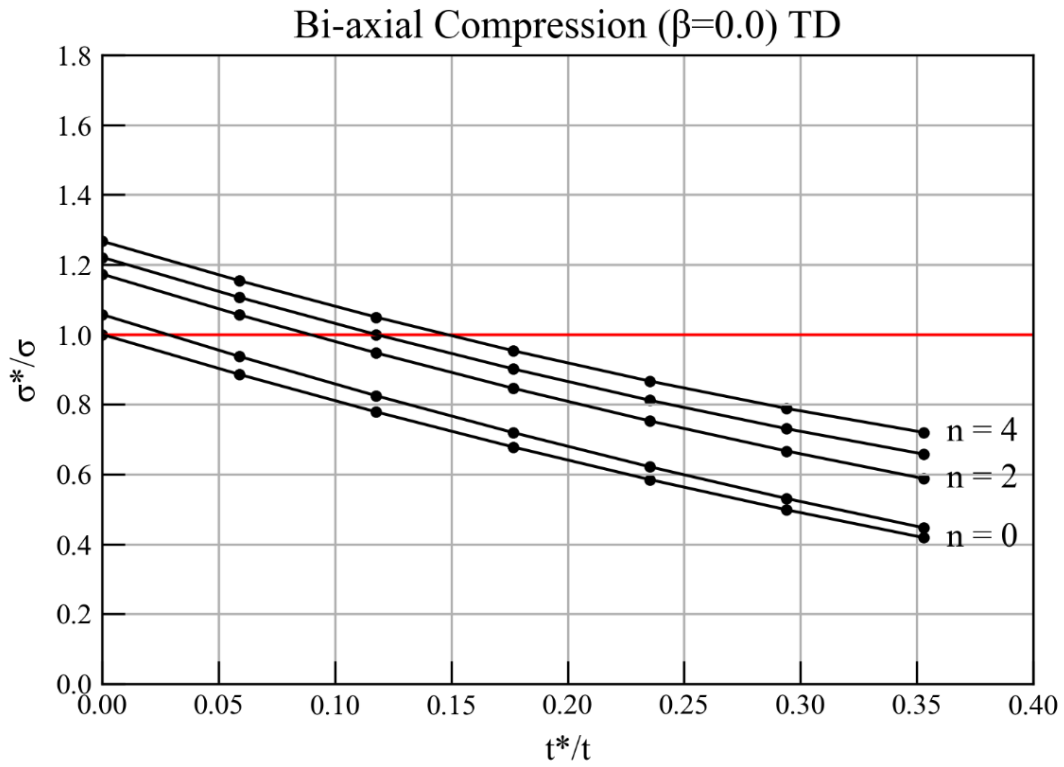


Figure 32. Reinforcement case: Bi-axial Compression ($\beta=0.0$) TD

Table 7. σ^*/σ values of reinforcement case: Bi-axial Compression ($\beta=0.0$) TD

t^*	$n = 1$	$n = 2$	$n = 3$	$n = 4$
0	1.057	1.173	1.221	1.267
1	0.937	1.056	1.106	1.154
2	0.825	0.947	1.000	1.050
3	0.719	0.846	0.902	0.954
4	0.621	0.753	0.812	0.867
5	0.531	0.666	0.730	0.788
6	0.447	0.588	0.658	0.720

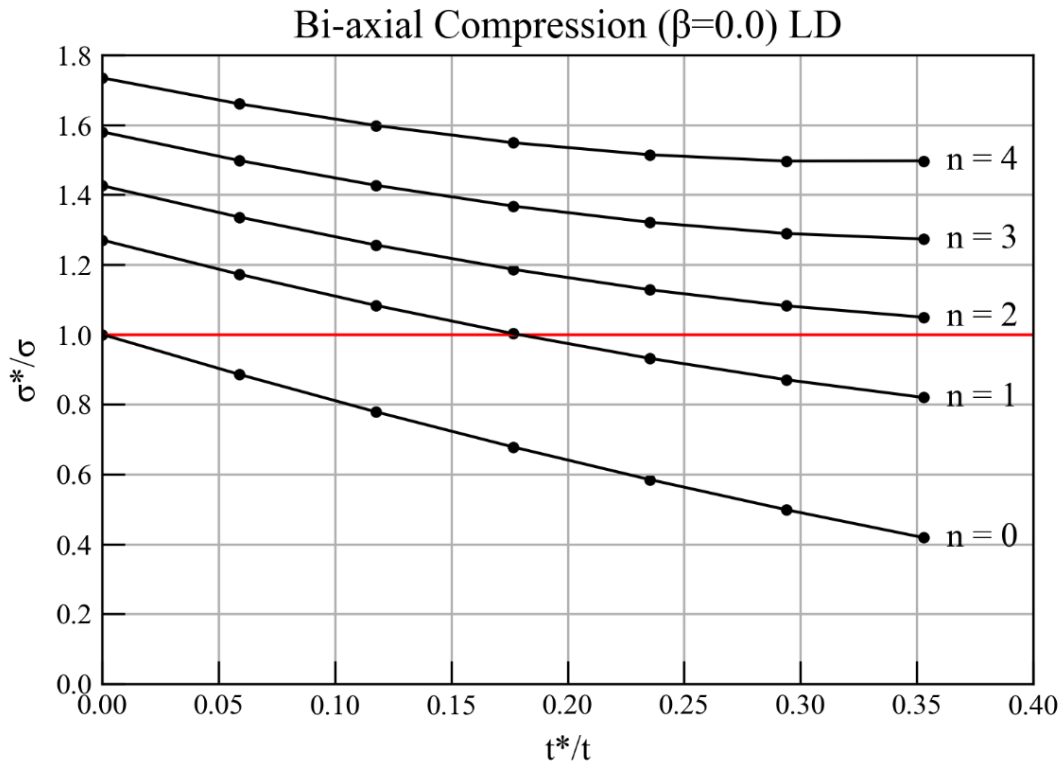


Figure 33. Reinforcement case: Bi-axial Compression ($\beta=0.0$) LD

Table 8. σ^*/σ values of reinforcement case: Bi-axial Compression ($\beta=0.0$) LD

t^*	$n = 1$	$n = 2$	$n = 3$	$n = 4$
0	1.270	1.426	1.580	1.734
1	1.172	1.336	1.498	1.660
2	1.083	1.256	1.427	1.598
3	1.003	1.186	1.368	1.549
4	0.932	1.128	1.321	1.514
5	0.870	1.082	1.289	1.496
6	0.820	1.049	1.273	1.497

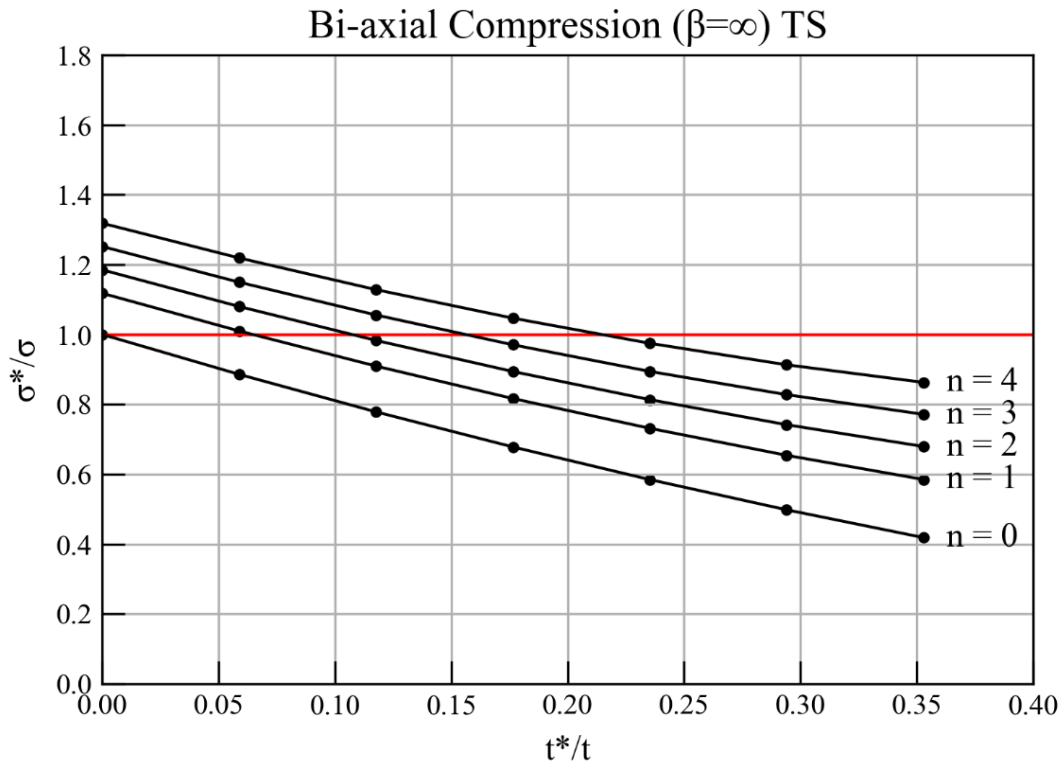


Figure 34. Reinforcement case: Bi-axial Compression ($\beta=\infty$) TS

Table 9. σ^*/σ values of reinforcement case: Bi-axial Compression ($\beta=\infty$) TS

t^*	$n = 1$	$n = 2$	$n = 3$	$n = 4$
0	1.118	1.185	1.252	1.318
1	1.010	1.080	1.150	1.219
2	0.910	0.983	1.056	1.128
3	0.817	0.894	0.971	1.047
4	0.731	0.814	0.894	0.975
5	0.654	0.742	0.828	0.913
6	0.585	0.679	0.772	0.863

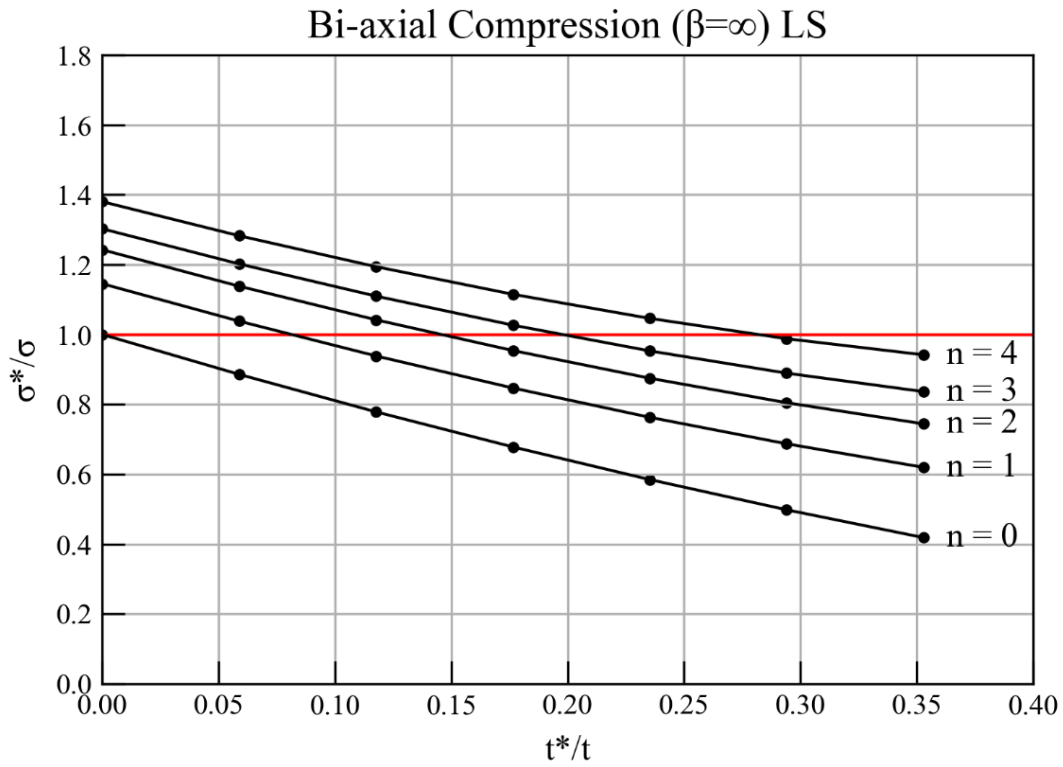


Figure 35. Reinforcement case: Bi-axial Compression ($\beta=\infty$) LS

Table 10. σ^*/σ values of reinforcement case: Bi-axial Compression ($\beta=\infty$) LS

t^*	$n = 1$	$n = 2$	$n = 3$	$n = 4$
0	1.145	1.242	1.302	1.380
1	1.038	1.138	1.202	1.283
2	0.939	1.042	1.110	1.194
3	0.847	0.954	1.027	1.115
4	0.763	0.875	0.953	1.046
5	0.687	0.805	0.889	0.988
6	0.620	0.744	0.837	0.942

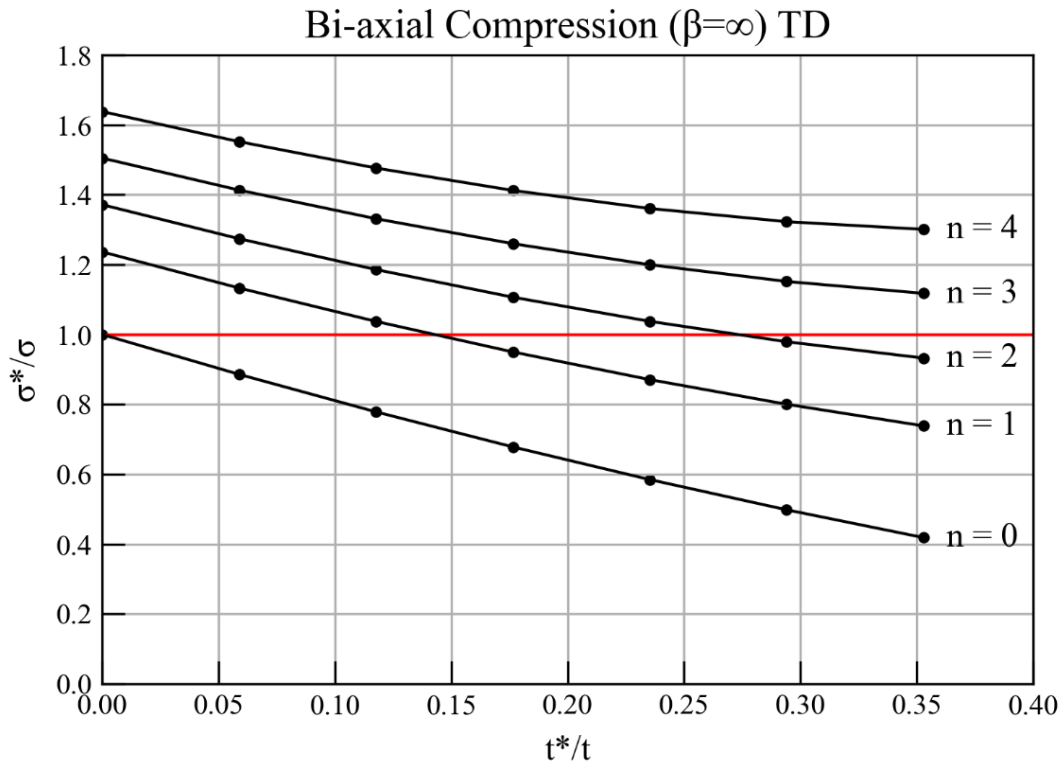


Figure 36. Reinforcement case: Bi-axial Compression ($\beta=\infty$) TD

Table 11. σ^*/σ values of reinforcement case: Bi-axial Compression ($\beta=\infty$) TD

t^*	$n = 1$	$n = 2$	$n = 3$	$n = 4$
0	1.236	1.371	1.505	1.638
1	1.133	1.274	1.413	1.552
2	1.037	1.186	1.331	1.476
3	0.950	1.107	1.260	1.412
4	0.871	1.038	1.200	1.361
5	0.800	0.979	1.152	1.323
6	0.738	0.933	1.118	1.301

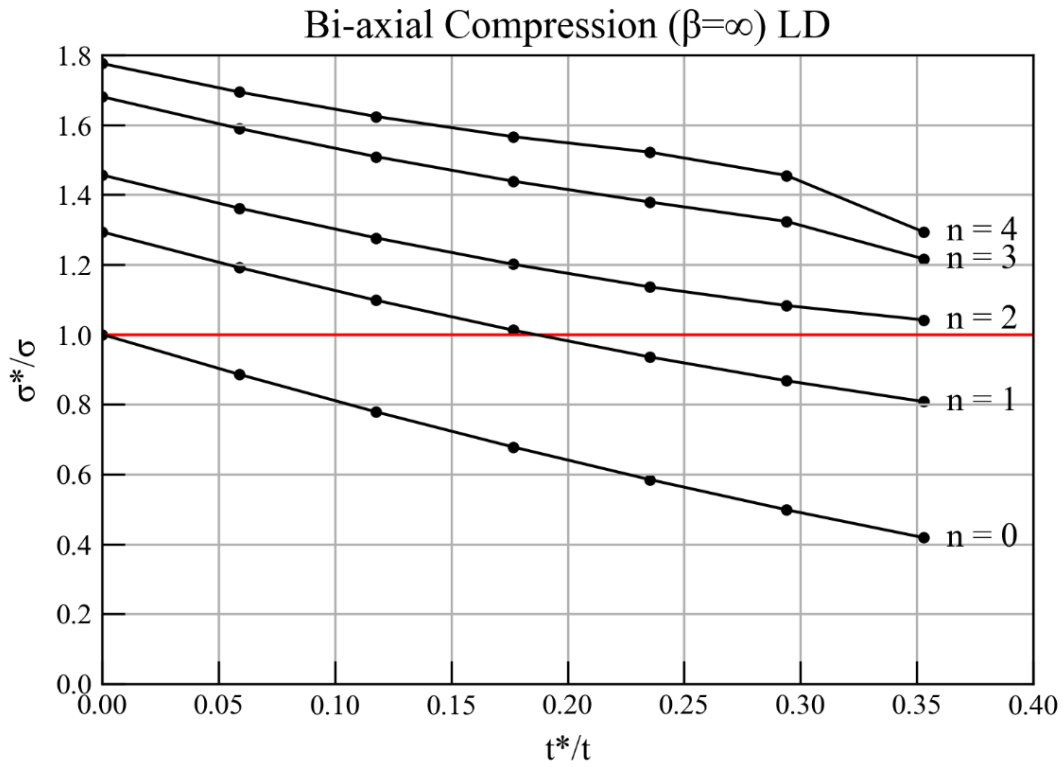


Figure 37. Reinforcement case: Bi-axial Compression ($\beta=\infty$) LD

Table 12. σ^*/σ values of reinforcement case: Bi-axial Compression ($\beta=\infty$) LD

t^*	$n = 1$	$n = 2$	$n = 3$	$n = 4$
0	1.293	1.456	1.680	1.775
1	1.192	1.362	1.590	1.694
2	1.098	1.276	1.509	1.624
3	1.013	1.201	1.439	1.566
4	0.936	1.136	1.379	1.522
5	0.868	1.083	1.323	1.455
6	0.808	1.042	1.217	1.294

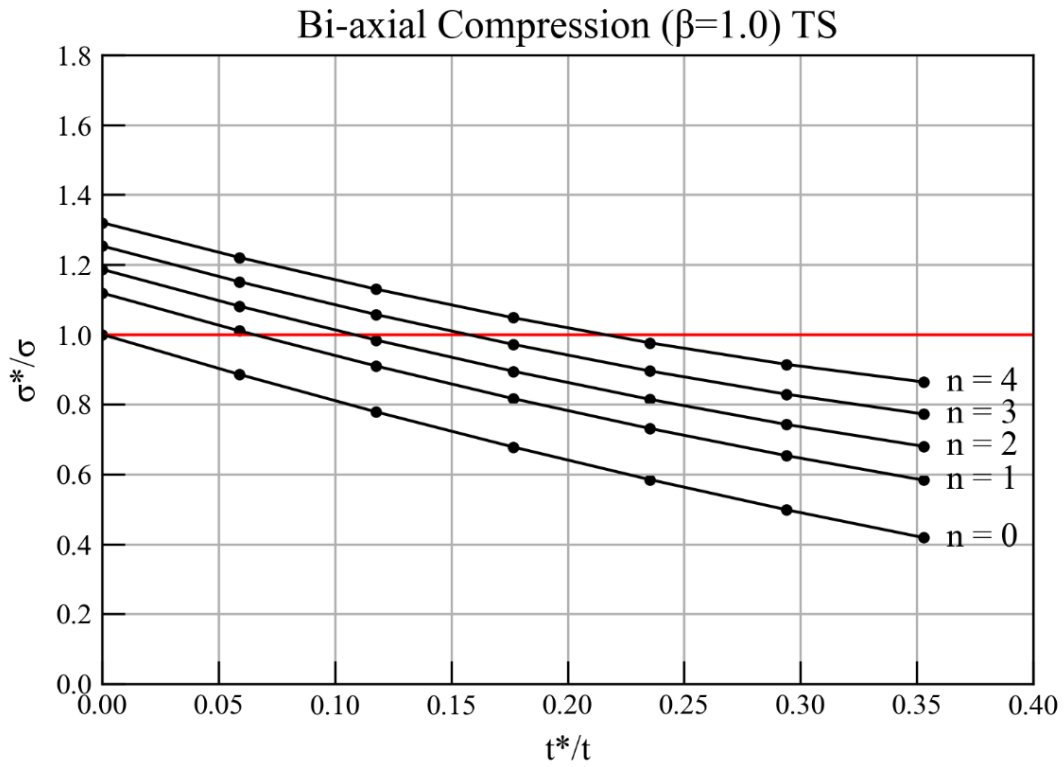


Figure 38. Reinforcement case: Bi-axial Compression ($\beta=1.0$) TS

Table 13. σ^*/σ values of reinforcement case: Bi-axial Compression ($\beta=1.0$) TS

t^*	$n = 1$	$n = 2$	$n = 3$	$n = 4$
0	1.119	1.186	1.253	1.320
1	1.011	1.081	1.151	1.221
2	0.910	0.984	1.057	1.130
3	0.817	0.895	0.972	1.048
4	0.731	0.814	0.896	0.976
5	0.653	0.742	0.829	0.914
6	0.583	0.680	0.772	0.864

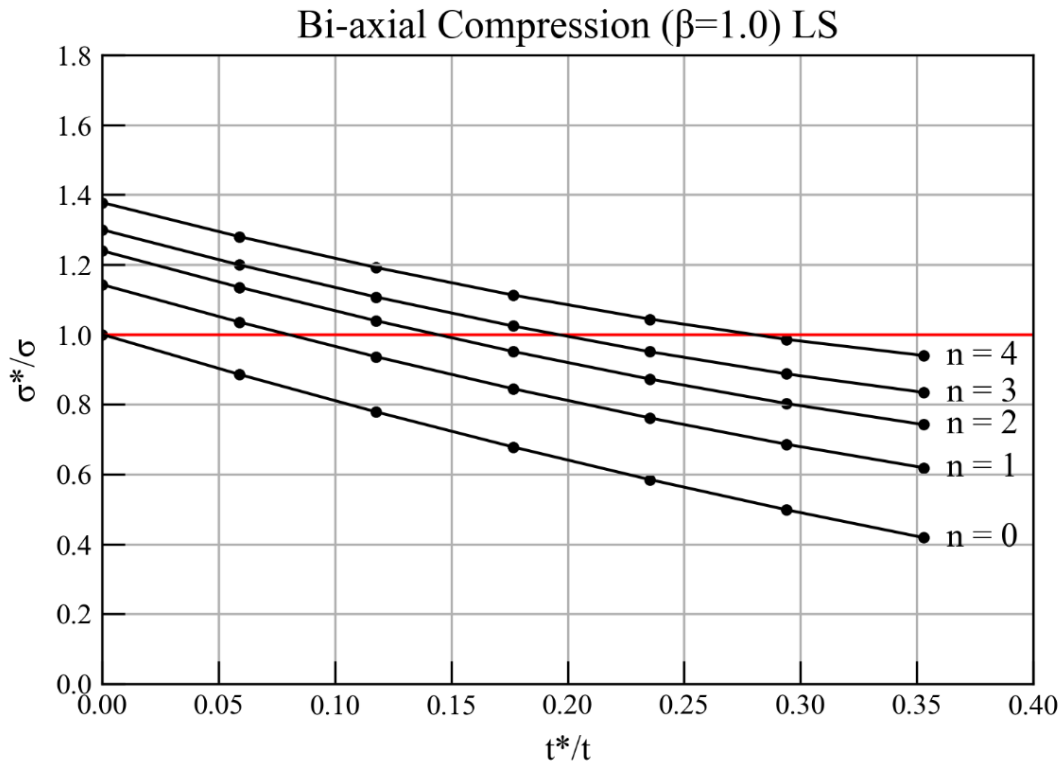


Figure 39. Reinforcement case: Bi-axial Compression ($\beta=1.0$) LS

Table 14. σ^*/σ values of reinforcement case: Bi-axial Compression ($\beta=1.0$) LS

t^*	$n = 1$	$n = 2$	$n = 3$	$n = 4$
0	1.143	1.239	1.300	1.378
1	1.036	1.135	1.199	1.280
2	0.936	1.039	1.107	1.192
3	0.845	0.952	1.024	1.113
4	0.761	0.872	0.951	1.044
5	0.686	0.802	0.887	0.986
6	0.619	0.742	0.834	0.940

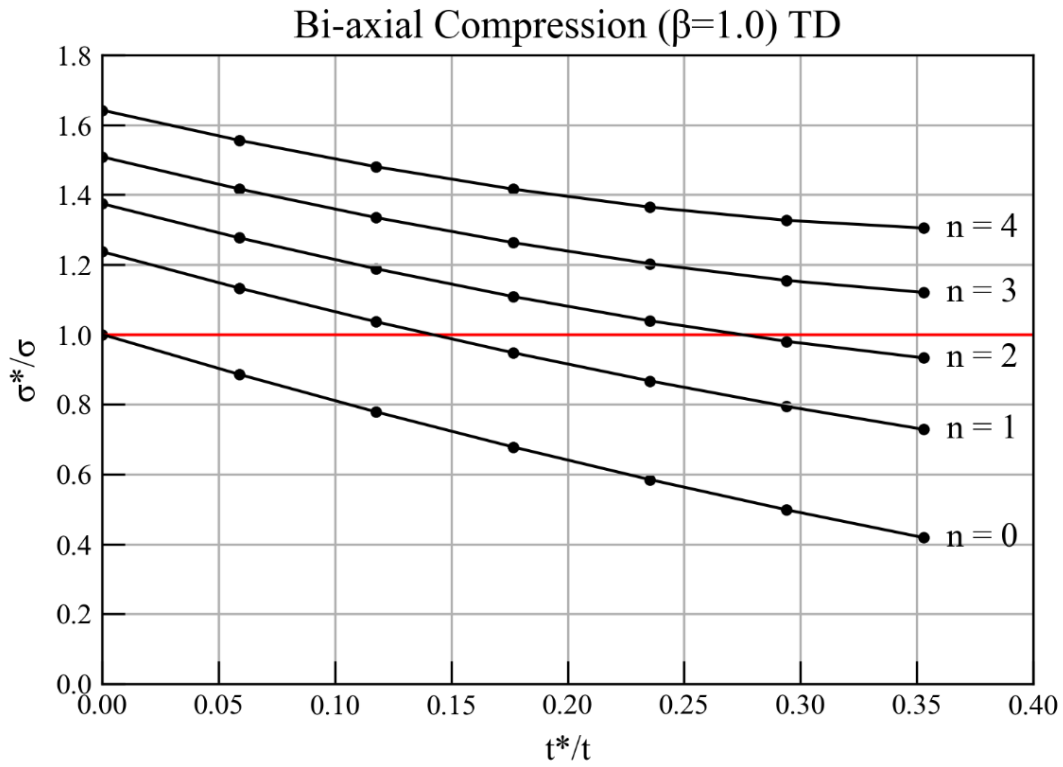


Figure 40. Reinforcement case: Bi-axial Compression ($\beta=1.0$) TD

Table 15. σ^*/σ values of reinforcement case: Bi-axial Compression ($\beta=1.0$) TD

t^*	$n = 1$	$n = 2$	$n = 3$	$n = 4$
0	1.237	1.374	1.508	1.642
1	1.133	1.277	1.417	1.556
2	1.036	1.188	1.335	1.480
3	0.948	1.109	1.263	1.416
4	0.867	1.039	1.203	1.364
5	0.794	0.980	1.155	1.327
6	0.729	0.933	1.120	1.305

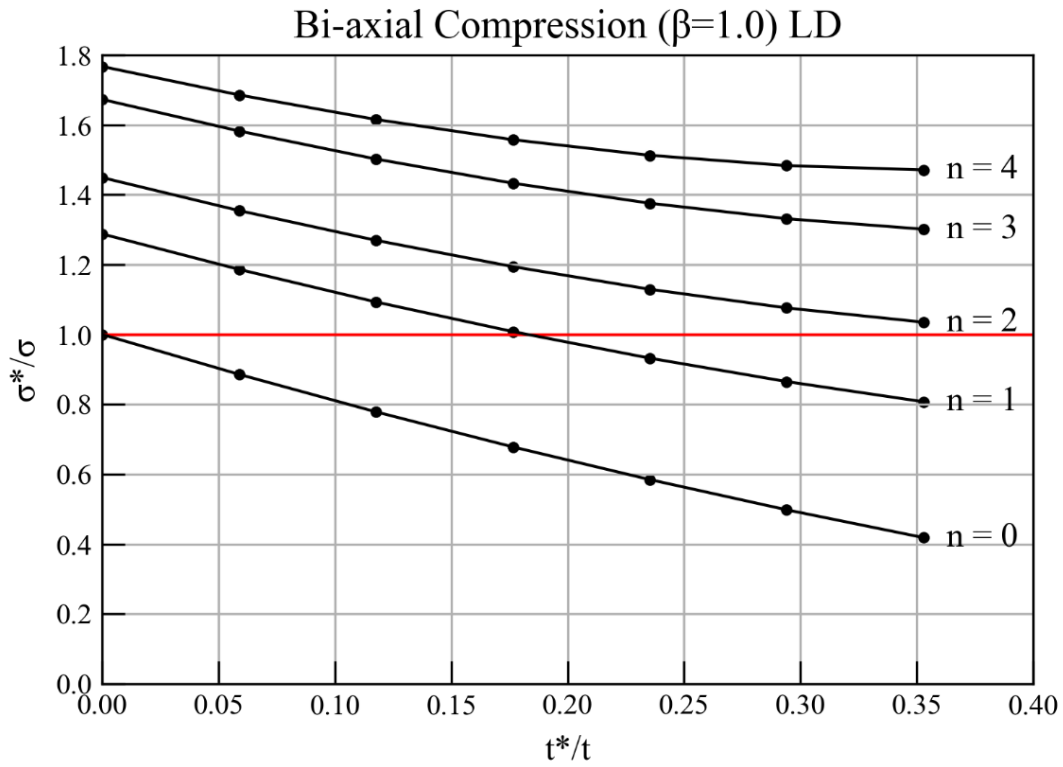


Figure 41. Reinforcement case: Bi-axial Compression ($\beta=1.0$) LD

Table 16. σ^*/σ values of reinforcement case: Bi-axial Compression ($\beta=1.0$) LD

t^*	$n = 1$	$n = 2$	$n = 3$	$n = 4$
0	1.288	1.449	1.673	1.767
1	1.186	1.355	1.582	1.686
2	1.093	1.269	1.502	1.615
3	1.008	1.194	1.433	1.557
4	0.932	1.129	1.376	1.513
5	0.865	1.076	1.331	1.483
6	0.807	1.035	1.301	1.471

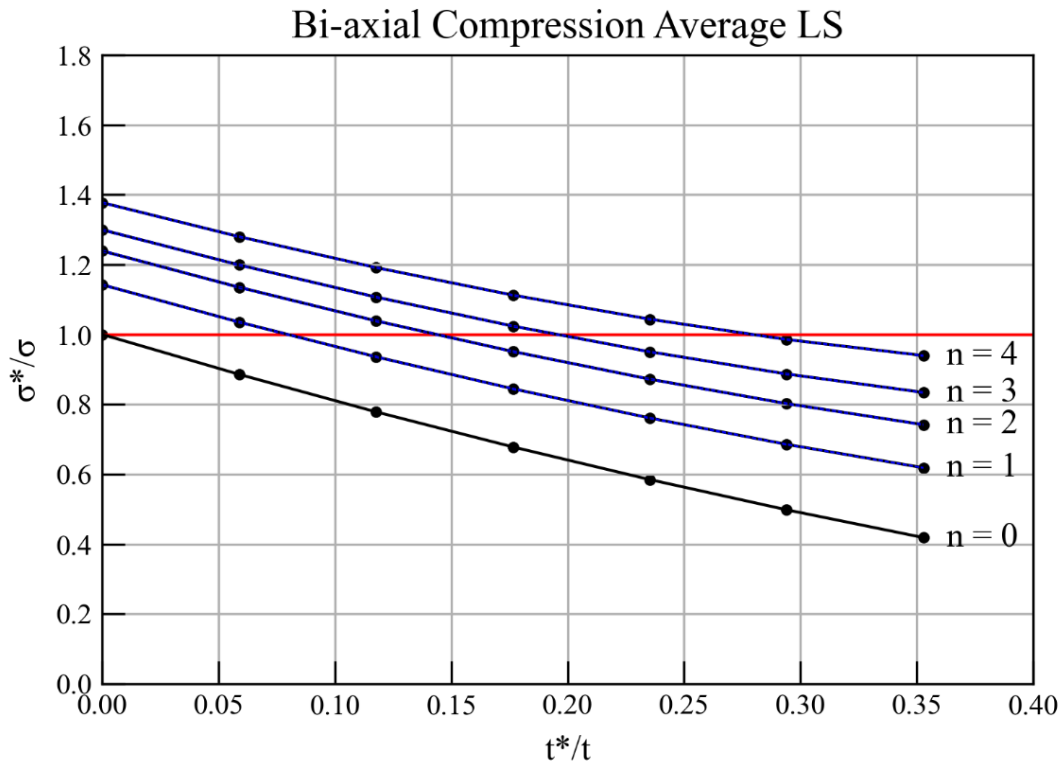


Figure 42. Reinforcement case: Bi-axial Compression Average LS

Table 17. σ^*/σ average values and standard deviations of reinforcement case: Bi-axial Average ($\beta=1.0$) LS

t*	n = 1	n = 2	n = 3	n = 4
0	1.142	1.239	1.300	1.377
1	1.035	1.135	1.199	1.280
2	0.936	1.039	1.107	1.192
3	0.845	0.951	1.024	1.113
4	0.761	0.872	0.951	1.044
5	0.686	0.802	0.887	0.986
6	0.619	0.742	0.834	0.940
Sample Standard Deviation				
0	1.52E-03	1.72E-03	1.55E-03	1.44E-03
1	1.42E-03	1.64E-03	1.48E-03	1.37E-03
2	1.30E-03	1.56E-03	1.42E-03	1.31E-03
3	1.18E-03	1.47E-03	1.36E-03	1.26E-03
4	1.05E-03	1.40E-03	1.30E-03	1.21E-03
5	8.95E-04	1.32E-03	1.25E-03	1.16E-03
6	6.97E-04	1.24E-03	1.21E-03	1.13E-03

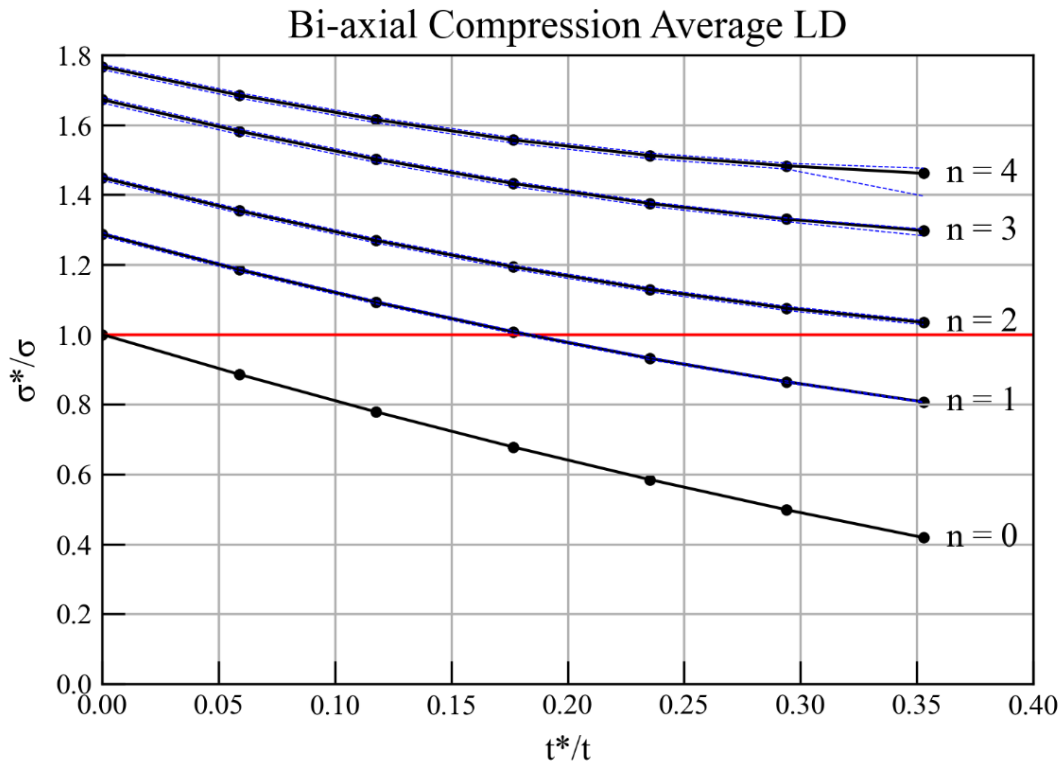


Figure 43. Reinforcement case: Bi-axial Compression Average LD

Table 18. σ^*/σ average values and standard deviations of reinforcement case: Bi-axial Average ($\beta=1.0$) LD

t^*	$n = 1$	$n = 2$	$n = 3$	$n = 4$
0	1.287	1.449	1.672	1.766
1	1.186	1.354	1.582	1.685
2	1.093	1.269	1.501	1.615
3	1.008	1.194	1.432	1.557
4	0.932	1.129	1.375	1.512
5	0.865	1.076	1.330	1.483
6	0.807	1.035	1.297	1.461
Sample Standard Deviation				
0	3.36E-03	4.08E-03	5.07E-03	4.71E-03
1	3.14E-03	3.99E-03	4.91E-03	4.74E-03
2	2.90E-03	3.92E-03	4.75E-03	4.79E-03
3	2.61E-03	3.86E-03	4.55E-03	4.89E-03
4	2.25E-03	3.82E-03	4.23E-03	5.03E-03
5	1.75E-03	3.79E-03	3.54E-03	5.25E-03
6	1.01E-03	3.75E-03	6.16E-03	2.49E-02

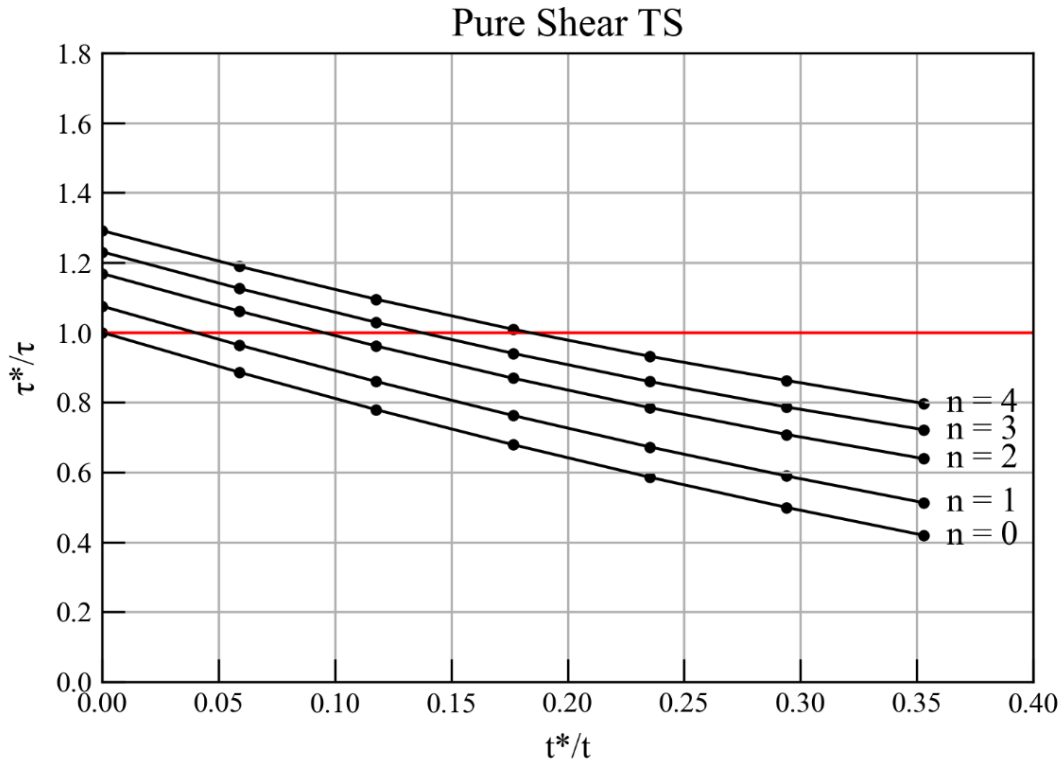


Figure 44. Reinforcement case: Pure Shear TS

Table 19. σ^*/σ values of reinforcement case: Pure Shear TS

t^*	$n = 1$	$n = 2$	$n = 3$	$n = 4$
0	1.075	1.169	1.231	1.291
1	0.964	1.061	1.126	1.189
2	0.860	0.961	1.029	1.095
3	0.763	0.869	0.940	1.009
4	0.672	0.785	0.859	0.932
5	0.589	0.708	0.787	0.863
6	0.513	0.639	0.722	0.797

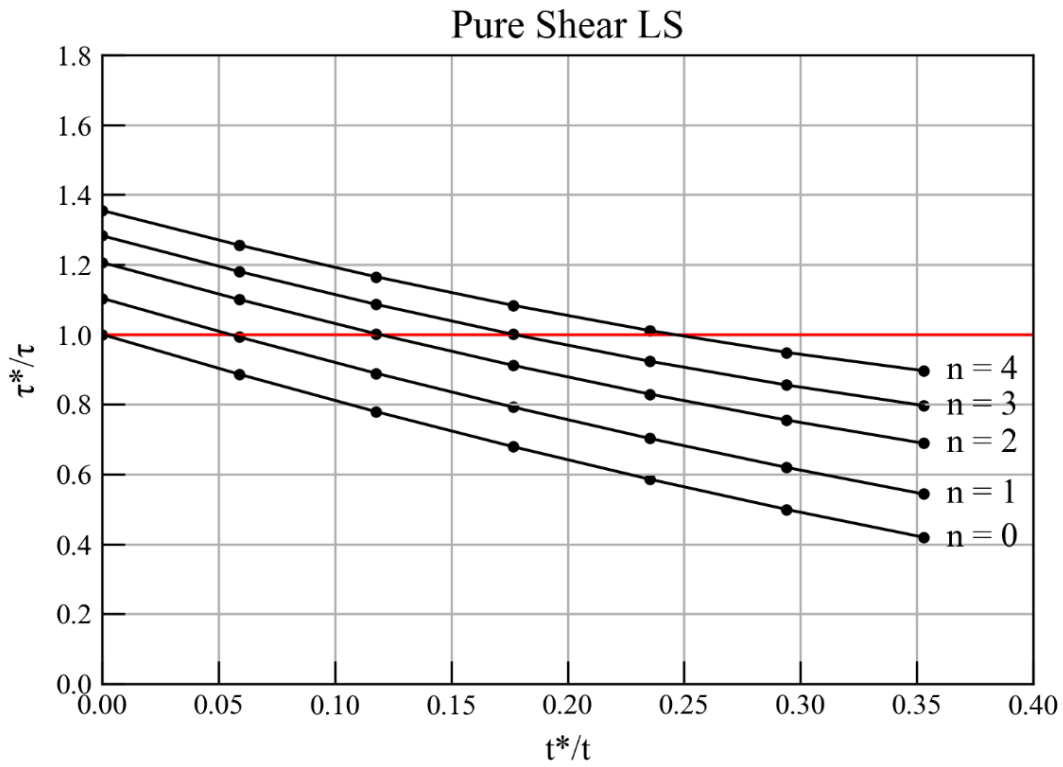


Figure 45. Reinforcement case: Pure Shear LS

Table 20. σ^*/σ values of reinforcement case: Pure Shear LS

t^*	$n = 1$	$n = 2$	$n = 3$	$n = 4$
0	1.104	1.206	1.283	1.355
1	0.993	1.100	1.180	1.256
2	0.889	1.002	1.086	1.165
3	0.792	0.912	1.000	1.083
4	0.702	0.829	0.923	1.011
5	0.620	0.755	0.855	0.949
6	0.543	0.689	0.797	0.896

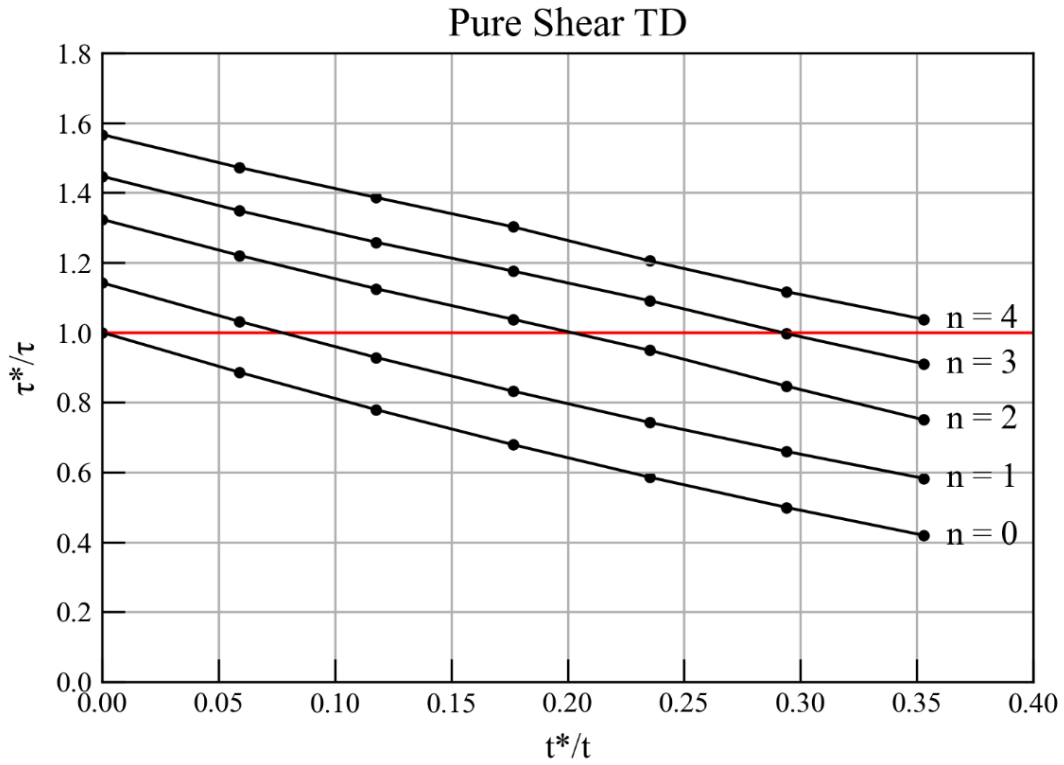


Figure 46. Reinforcement case: Pure Shear TD

Table 21. σ^*/σ values of reinforcement case: Pure Shear TD

t^*	$n = 1$	$n = 2$	$n = 3$	$n = 4$
0	1.142	1.324	1.447	1.566
1	1.032	1.221	1.349	1.472
2	0.929	1.125	1.258	1.386
3	0.832	1.038	1.176	1.302
4	0.743	0.949	1.091	1.205
5	0.659	0.846	0.997	1.117
6	0.583	0.750	0.911	1.038

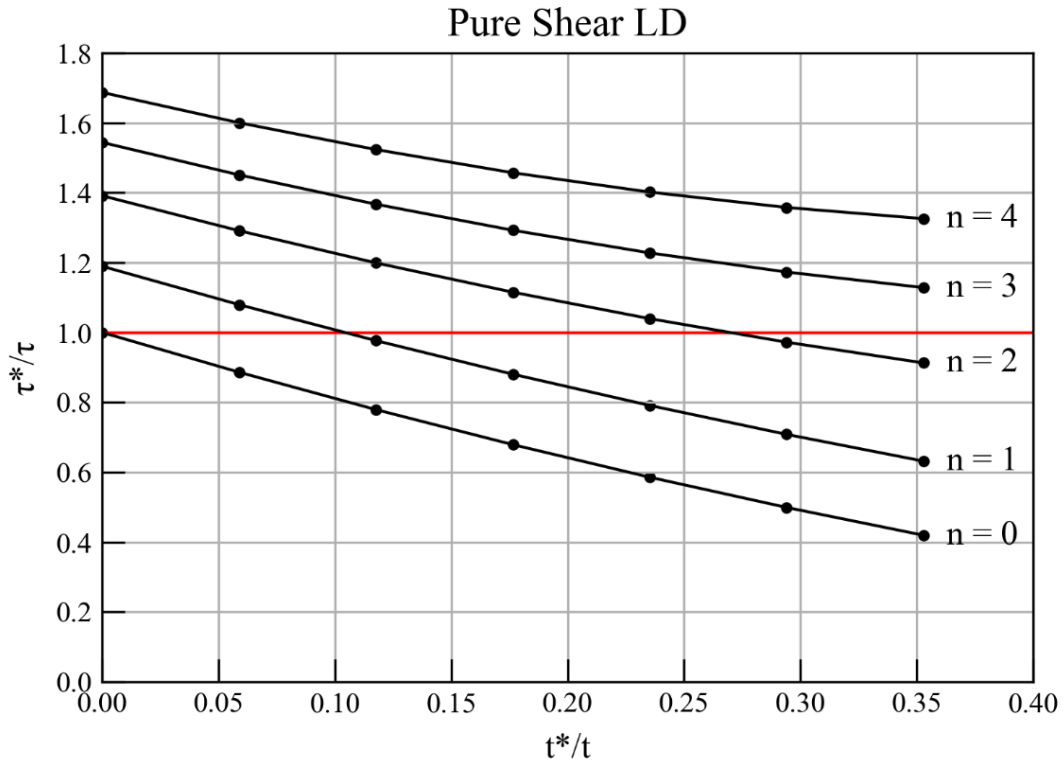


Figure 47. Reinforcement case: Pure Shear LD

Table 22. σ^*/σ values of reinforcement case: Pure Shear LD

t*	n = 1	n = 2	n = 3	n = 4
0	1.189	1.391	1.544	1.687
1	1.080	1.291	1.451	1.600
2	0.977	1.199	1.367	1.523
3	0.881	1.115	1.293	1.457
4	0.791	1.040	1.228	1.402
5	0.708	0.972	1.173	1.358
6	0.632	0.913	1.128	1.326

The FEA results lead to a number of conclusions about the reinforcement arrangement used in this analysis.

Since the FRP stiffeners are relatively weak in comparison with the steel plate, the expected failure mode of the reinforced plate is overall collapse. The stiffeners buckle with the plate following its surface curvature.

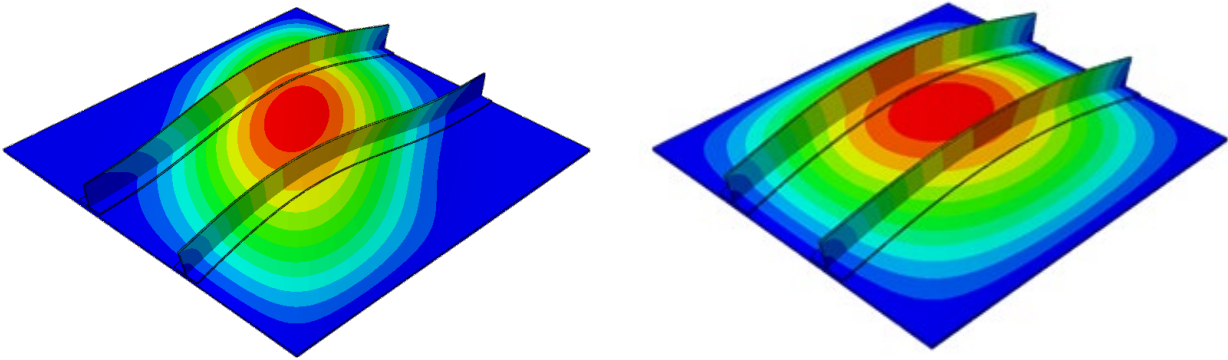


Figure 48. Fundamental modes of composite reinforced plates in pure shear (left) and bi-axial compression (right)

In some cases, a mode different from the fundamental appears. This mode switch is observed through the $\sigma^*/\sigma - t^*/t$ curves as a discontinuity of the curve’s slope. The main reasons for this are:

- The stiffener number or/and stiffness are above a certain value
- The plate’s thickness to breadth ratio is below a certain value
- The main load is perpendicular to the stiffeners
- The stiffener is placed to a region close to a nodal line of the next mode

The switch almost always happens as a combination of the above. The slope discontinuity point cannot be predicted without further analysis on the topic. This adds an uncertainty to any attempt to interpolate data from the FEA model but its effect is ignored as it is considered small.

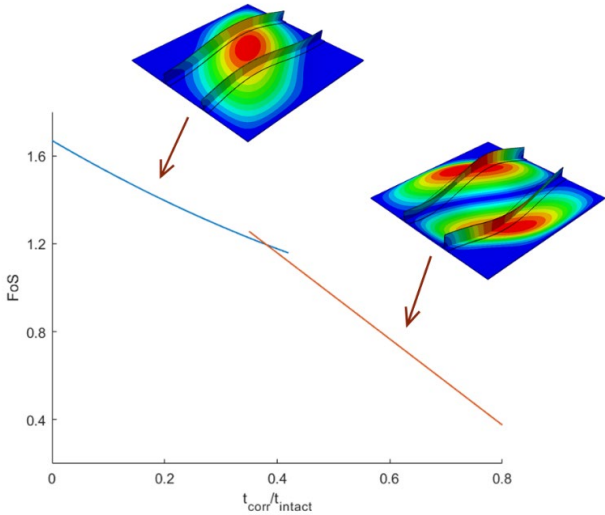


Figure 49. Mode switch effect on the stress-thickness curve

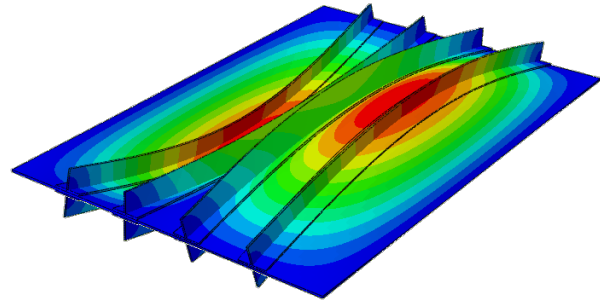
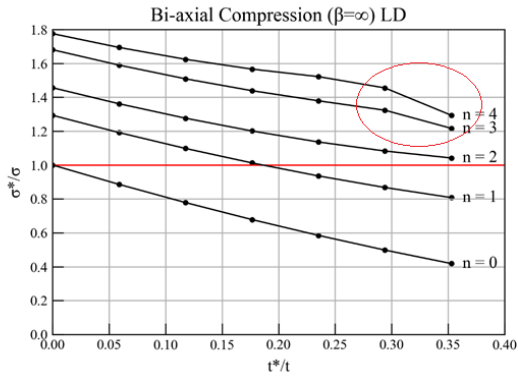


Figure 50. Case of mode switch in bi-axial compression for $\beta = \infty$

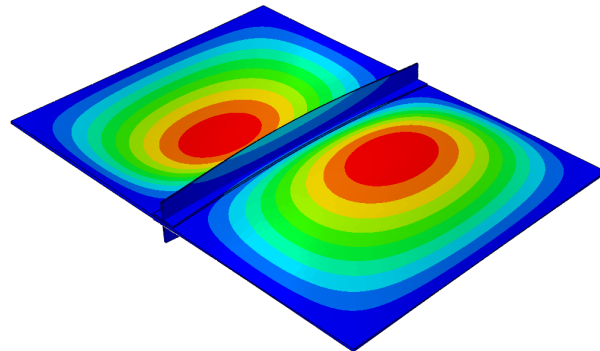
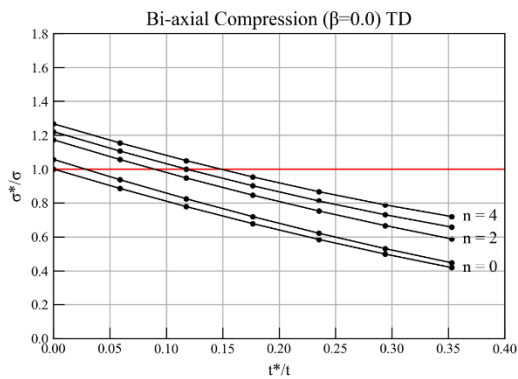


Figure 51. Case of initial mode switch in bi-axial compression for $\beta = 0.0$

Based on the results, the following were observed:

- The critical buckling value of a longitudinal reinforcement are higher than a transverse reinforcement's with the same parameters
- The critical buckling value of a reinforcement arrangement is lowest for the case of pure shear

The above lead to the conclusions:

- Longitudinal reinforcement is preferred
- Design against pure shear is sufficient for all cases

5 Probabilistic Approach

A probabilistic model was created in order to calculate the amplitude of rehabilitation that a type of reinforcement provides to a plate of any dimension. Five different plates were chosen to produce the model and 9 different plates to test the model.

5.1 Model fitting

5.1.1 CCD

The model is a Face-centered CCD. The response of the CCD is the Factor of Safety (FoS) against linear elastic buckling provided by the repair method. Its formula is:

$$FoS = \frac{\tau^*}{\tau}$$

with:

- τ^* : the critical buckling value of the repaired corroded plate in pure shear
- τ : the critical buckling value of the intact unreinforced plate in pure shear

The design constants are:

- Plate: Steel / $E = 210 \text{ GPa}$ / $\nu = 0.3$
- Stiffener: GFRP / T-beam / $b_{\text{flange}} = 150 \text{ mm}$ / $t = 9.5 \text{ mm}$
- Longitudinal single-sided reinforcement with two equi-distant stiffeners

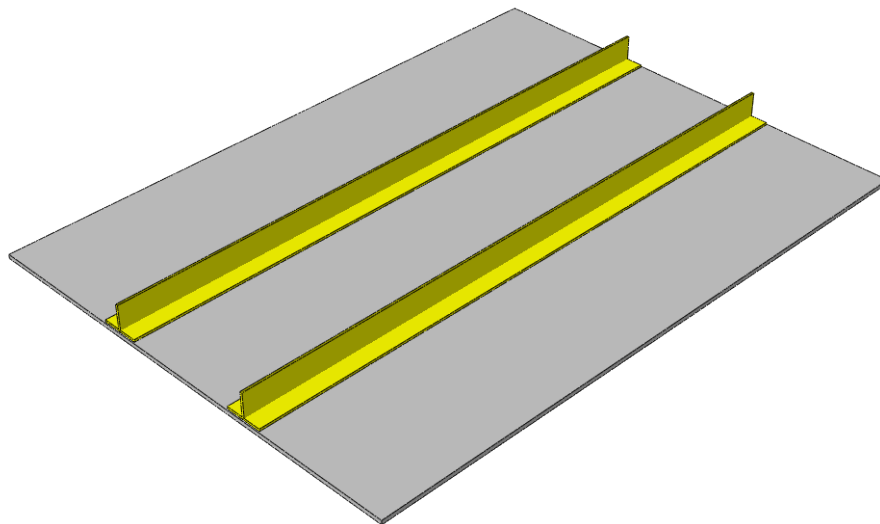


Figure 52. Reinforcement arrangement of the probabilistic approach

Table 23. CCD Factors

Factors	Formula	Low Level [-1]	Mid Level [0]	High Level [+1]
Relative web height	$h_{\text{web}}/(t-t^*)$	6	9	12
% of corrosion	$t^*/t \cdot 100\%$	0	15	30

5.1.2 CLT

The CCD model is created by multiple plates, that leads to the CCD point having multiple responses. So the need of a point estimator arises to reduce the multiple points to one. The method chosen to estimate the points is the CLT. For each point a one-tailed 99% interval of confidence with lower bound is calculated with the use of Student's T distribution. The mathematical meaning behind this concept is:

There is a 99% probability that the interval $[L, +\infty)$ includes the population mean, or:

$$P[L \leq \mu < +\infty] = 0.99$$

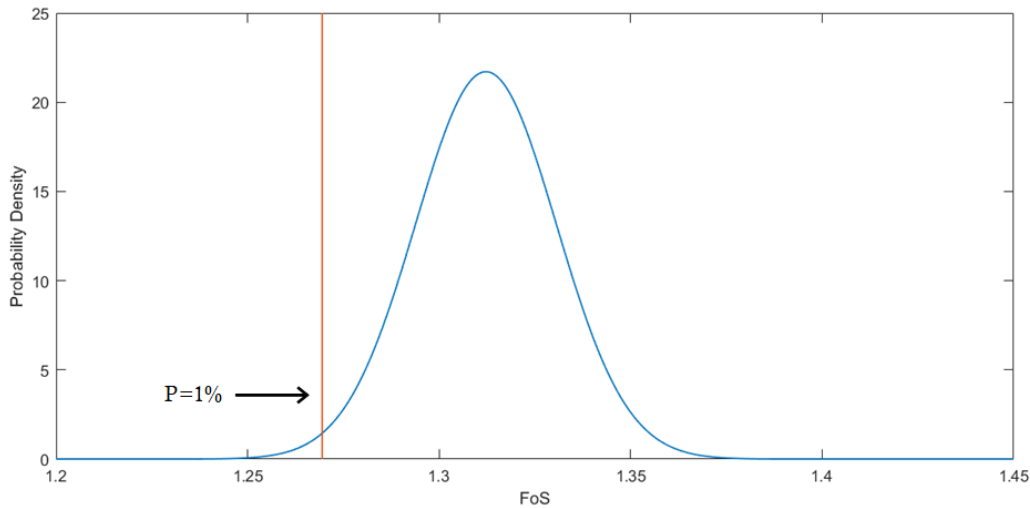


Figure 53. Lower bound example of one-tailed confidence interval

L is the estimated point used in the CCD. More specifically:

$$FoS_{ij} = L_{ij} = m_{ij} - t_{0.01}(n) \frac{S_{ij}}{\sqrt{n}}$$

where:

- m_{ij} : the sample mean
- S_{ij} : the sample standard deviation
- n : the number of plates
- $t_{0.01}(n)$: the t-value taken from a Student's T distribution table

Five plates of different dimensions were chosen to cover a variety of aspect ratios and thicknesses used in ship structural design. 9 simulations were ran for each plate to cover all CCD points.

Table 24. Fitting model plate properties

Plate Number	[1]	[2]	[3]	[4]	[5]
Length [mm]	2000	2500	1600	1600	1000
Width [mm]	2000	2300	1380	1290	750
Thick. [mm]	17	16	13	14.5	16

Table 25. FEA results for CCD

Points	Plate [1]	Plate [2]	Plate [3]	Plate [4]	Plate [5]	m_{ij}	S_{ij}	FoS _{ij}
(-1,-1)	1.296	1.264	1.376	1.322	1.304	1.312	0.041	1.250
(-1,0)	0.969	0.938	1.040	0.997	0.999	0.989	0.038	0.931
(-1,+1)	0.686	0.659	0.749	0.715	0.733	0.708	0.036	0.654
(0,-1)	1.574	1.550	1.694	1.585	1.462	1.573	0.083	1.448
(0,0)	1.207	1.173	1.312	1.225	1.149	1.213	0.062	1.120
(0,+1)	0.878	0.841	0.967	0.902	0.870	0.892	0.048	0.820
(+1,-1)	1.869	1.887	2.032	1.861	1.599	1.850	0.157	1.614
(+1,0)	1.470	1.462	1.612	1.475	1.286	1.461	0.116	1.287
(+1,+1)	1.094	1.073	1.219	1.116	1.001	1.101	0.079	0.981

5.1.3 RSM

A quadratic response surface was fitted to the CCD points with MATLAB Curve Fitting Toolbox:

$$\eta = \beta_0 + \beta_1 x_1 + \beta_2 x_2 + \beta_{11} x_1^2 + \beta_{22} x_2^2 + \beta_{12} x_1 x_2, \quad 6 \leq x_1 \leq 12, \quad 0 \leq x_2 \leq 30$$

with $R^2 = 0.9999$ and $RMSE = 0.005448$.

Table 26. Response surface coefficients

β_0	β_1	β_2	β_{11}	β_{22}	β_{12}
0.8062	0.08056	-0.02089	-0.001079	6.816e-05	-0.0001996

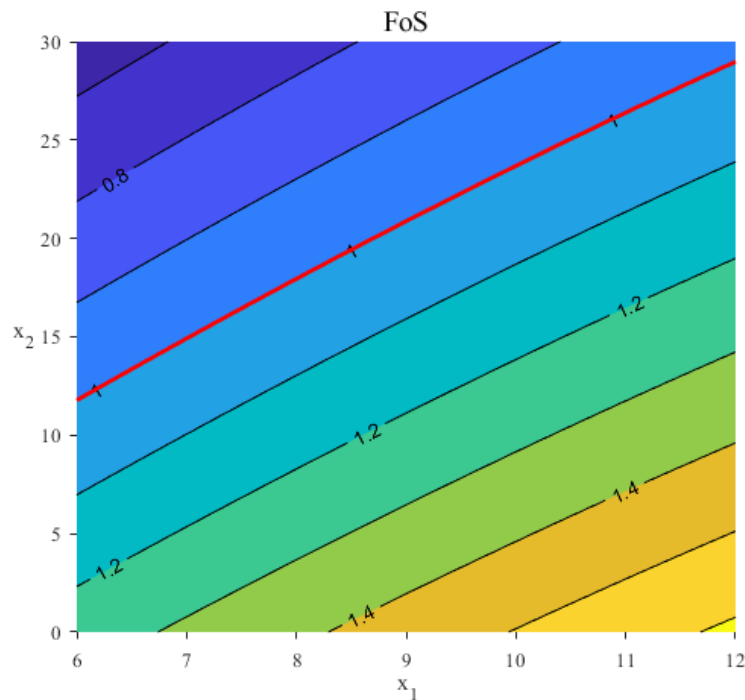
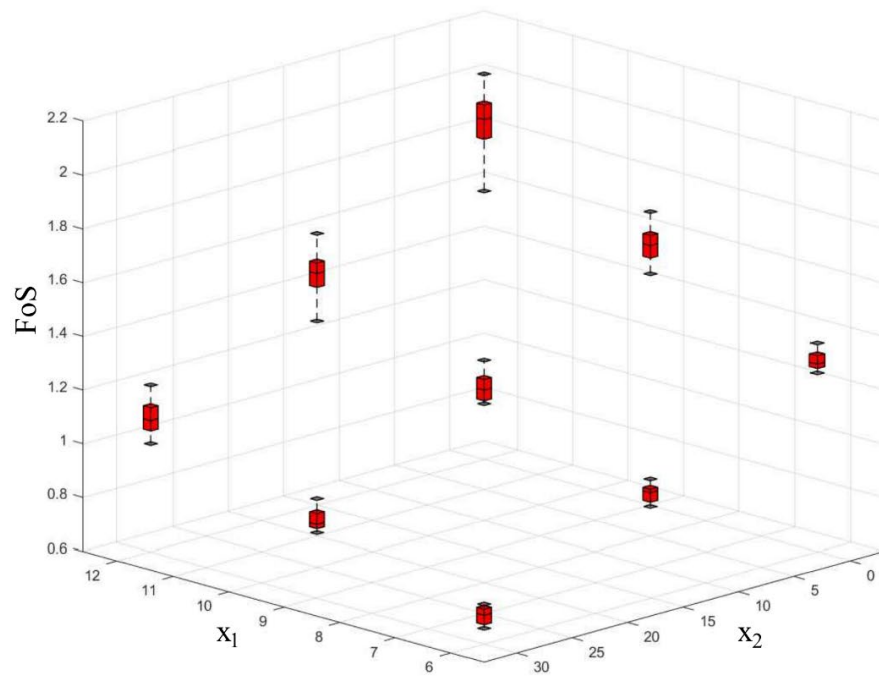


Figure 54. RSM contour



CLT
↓

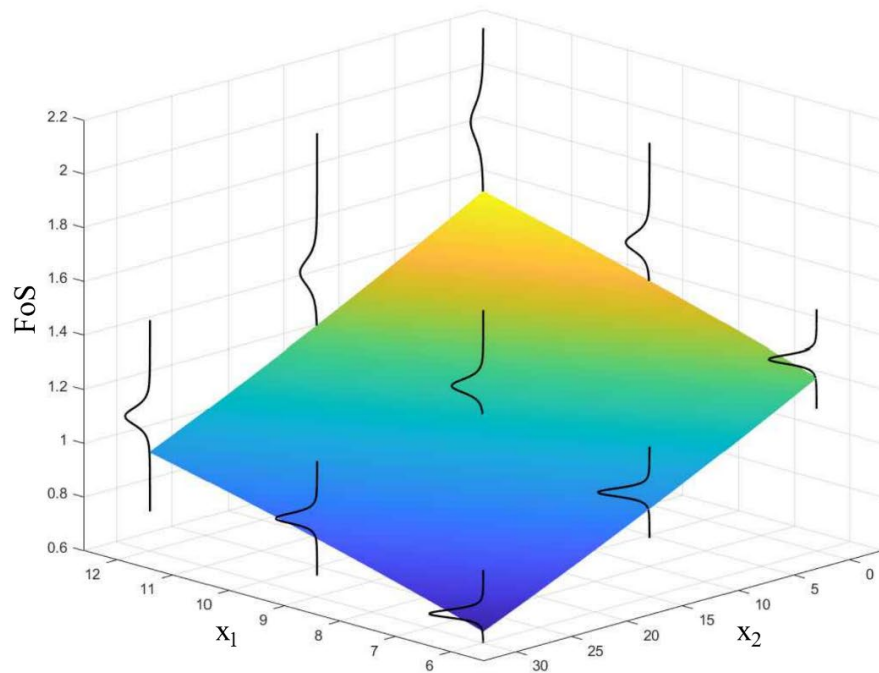


Figure 55. Creation of the probabilistic model with the use of CLT

5.2 Model testing

The 9 plates used for the testing phase along with their stiffeners are presented in Table 27. The plates' properties were inserted in the FEA simulation and the RSM model and the results were compared in Table 28. Plates with greater FoS_{FEA} are in the safe area above the response surface, meaning that the response surface underestimates their FoS and the repair design would be adequate.

Table 27. Testing phase plate dimensions

Plate	a [mm]	b [mm]	t [mm]	t* [mm]	h _{web} [mm]
(i)	2061	1718	15.4	4.5	129
(ii)	1539	1221	16.1	2.3	165
(iii)	1439	1358	13.9	1.0	111
(iv)	1950	1477	17.0	1.4	135
(v)	1295	1012	17.4	2.3	105
(vi)	1549	1280	15.0	1.8	123
(vii)	1039	781	16.6	2.7	155
(viii)	2151	1707	13.2	3.0	112
(ix)	2270	2027	15.6	0.2	170

Table 28. Test plates RSM and FEA results comparison

Plate	x_1	x_2	FoS_{RSM}	FoS_{FEA}	$FoS_{FEA} - Fos_{RSM}$
(i)	29%	11.798	0.990	1.079	0.090
(ii)	14%	11.917	1.301	1.388	0.087
(iii)	7%	8.587	1.263	1.468	0.205
(iv)	8%	8.632	1.245	1.238	-0.007
(v)	13%	6.936	1.035	1.047	0.012
(vi)	12%	9.318	1.200	1.315	0.115
(vii)	16%	11.116	1.216	1.200	-0.016
(viii)	23%	11.019	1.068	1.215	0.147
(ix)	1%	11.008	1.539	1.744	0.205

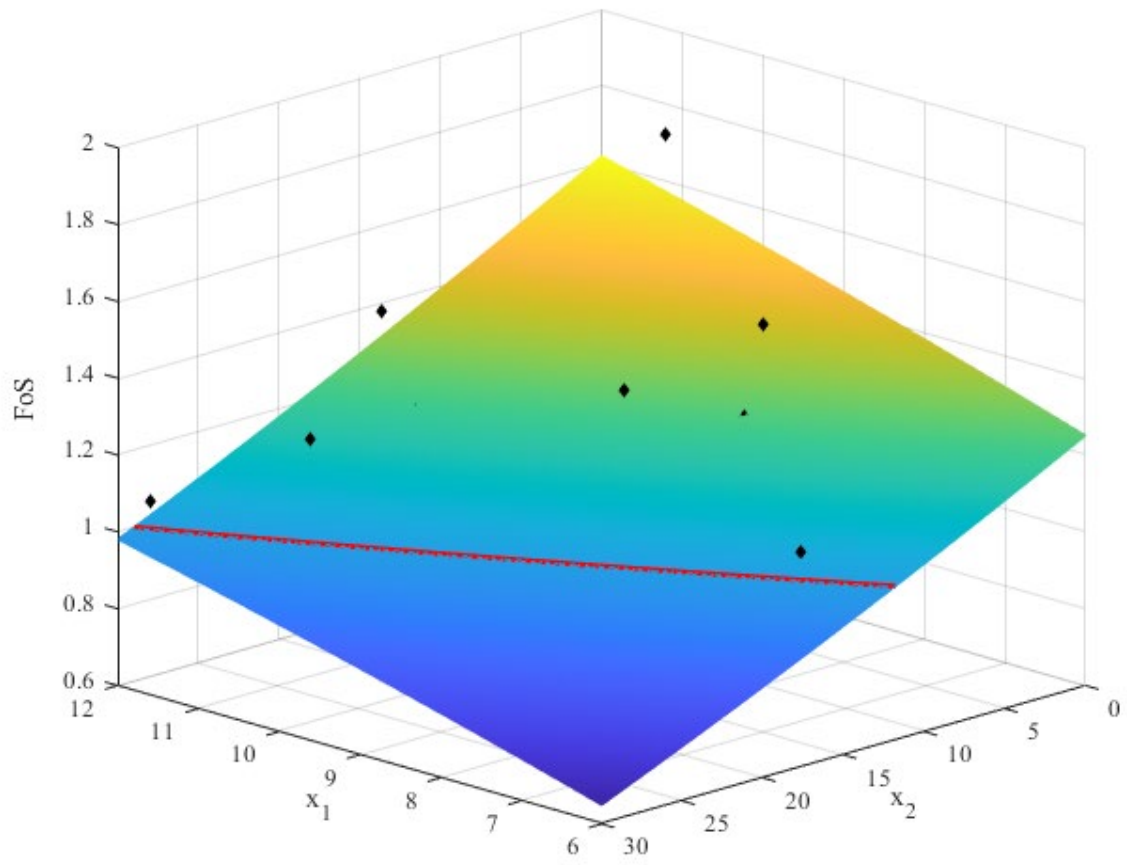


Figure 56. Test points in the RSM plot

6 Concluding Remarks

Material wastage due to uniform corrosion has proven to be a troubling issue in the maritime industry leading to great risks for the wellbeing of a ship. In this study, a new method of repair against buckling with the use of composite beams (FRP) was examined through FEA simulations. Even though composite beam reinforcement is light, in comparison with steel beam reinforcements, it gave adequate results for the case of repair against linear buckling. The probabilistic model introduced a repair design independent of the plate's dimensions with the only parameters being the plate's thickness before and after corrosion and the desired FoS.

Although the results of this method were positive, a lot of factors were not taken into consideration due to assumptions that were made in order to simplify the problem. In future works non-linear analysis FEA simulations can be extracted in order to test the reinforced plate's ultimate strength as well as non-linear effects such as plasticity and composite failure modes. Finally, the composite beam reinforcement should be thoroughly examined with laboratory experiments to check the accuracy of the FEA simulations.

References

- [1]. Common Structural Rules for Bulk Carriers and Oil Tankers, 01 Jan 2023
- [2]. Rec 76 IACS Guidelines for Surveys, Assessment and Repair of Hull Structure - Bulk Carriers - Rev.2 Corr.1 - Sept 2007
- [3]. Rec 96 Double Hull Oil Tankers - Guidelines for Surveys, Assessment and Repair of Hull Structures - Rev.1 May 2019 Clean
- [4]. Rec 84 Container Ships - Guidelines for Surveys, Assessment and Repair of Hull Structures - Rev.1 Nov 2017
- [5]. Anyfantis, K.N., 2019. Preliminary design assessment of an alternative repair method for corroded shear panels in ship hull structures. *Ocean engineering*, 188, p.106323.
- [6]. Karatzas, V.A., Kotsidis, E.A., Tsouvalis, N.G., 2015. Experimental fatigue study of composite patch repaired steel plates with cracks. *Appl. Compos. Mater.* 22 (5), 507–523
- [7]. Stein, M., Neff, J., 1947. Buckling stresses of simple supported rectangular flat plates in shear. NACA-TN-1222
- [8]. Montgomery, D.C., Runger, G.C., 2018. *Applied statistics and probability for engineers*. 7th edition. Wiley, New York
- [9]. Montgomery, D.C., 2000. *Design and analysis of experiments*. 5th edition. Wiley, New York
- [10]. Kasidit Chansawat, Tanarat Potisuk, Thomas H. Miller, Solomon C. Yim, Damian I. Kachlakev, "FE Models of GFRP and CFRP Strengthening of Reinforced Concrete Beams", *Advances in Civil Engineering*, vol. 2009, Article ID 152196, 13 pages, 2009.